Available online at www.sciencedirect.com
SCIENCE DIRECT®
ELSEVIER
European Journal of Mechanics B/Fluids 24 (2005) 659–682
EUROPEAN JOURNAL OF MECHANICS B/FLUIDS

Wave transformation models with exact second-order transfer

H. Bredmose [a,*], Y. Agnon [b], P.A. Madsen [c], H.A. Schäffer [a]

[a] *DHI Water & Environment, Agern Allé 5, DK-2970 Hørsholm, Denmark*
[b] *Department of Civil and Environmental Engineering, Technion, Haifa 32000, Israel*
[c] *Department of Mechanical Engineering, Technical University of Denmark, Building 403, DK-2800 Kgs. Lyngby, Denmark*

Received 10 March 2004; received in revised form 24 November 2004; accepted 6 December 2004

Available online 24 June 2005

Abstract

Fully dispersive deterministic evolution equations for irregular water waves are derived. The equations are formulated in the complex amplitudes of an irregular, directional wave spectrum and are valid for waves propagating in directions up to ±90° from the main direction of propagation under the assumptions of weak nonlinearity, slowly varying depth and negligible reflected waves. A weak deviation from straight and parallel bottom contours is allowed for. No assumptions on the vertical structure of the velocity field is made and as a result, the equations possess exact second-order bichromatic transfer functions when comparing to the reference solution of a Stokes-type analysis. Introduction of the so-called 'resonance assumption' leads to the evolution equations of among others Agnon, Sheremet, Gonsalves and Stiassnie [Coastal Engrg. 20 (1993) 29–58]. For unidirectional waves, the bichromatic transfer functions of the 'resonant' models are found to have only small deviations in general from the reference solution. We demonstrate that the 'resonant' models can be solved efficiently using Fast Fourier Transforms, while this is not possible for the 'exact' models. Simulation results for unidirectional wave propagation over a submerged bar show that the new models provide a good improvement from linear theory with respect to wave shape. This is due to the quadratic terms, enabling a nonlinear description of shoaling and de-shoaling, including the release of higher harmonics after the bar. For these simulations, the similarity between the 'exact' and 'resonant' models is confirmed. A test case of shorter waves, however, shows that the amplitude dispersion can be quite over-predicted in the models. This behaviour is investigated and confirmed through a third-order Stokes-type perturbation analysis.

Keywords: Nonlinear wave transformation; Deterministic spectral modelling; Fully dispersive wave theory; Fast Fourier Transform; Bichromatic transfer; Amplitude dispersion

1. Introduction

When a wave field propagates over varying depth, the wave spectrum changes due to shoaling, refraction and nonlinear interactions. Numerous wave models can be used to model these effects, varying from solving the Navier–Stokes equations, allowing for a free surface, over Boussinesq modelling in the time domain, to simple linear shoaling calculations. For large wave fields of two horizontal dimensions, Navier–Stokes modelling is too computationally demanding and Boussinesq modelling still

* Corresponding author.
E-mail addresses: heb@dhi.dk (H. Bredmose), agnon@techunix.technion.ac.il (Y. Agnon), prm@mek.dtu.dk (P.A. Madsen), has@dhi.dk (H.A. Schäffer).

0997-7546/$ – see front matter
doi:10.1016/j.euromechflu.2005.05.001

requires an extensive computational effort. For practical use, there is thus an interest in computationally faster models, yet being more accurate than a simple linear wave shoaling calculation.

Evolution equations for the wave amplitudes of a complex wave spectrum represent a model class of this type. In such models, time periodicity of the wave field is assumed, allowing for expanding the wave field as a Fourier series in time. The Fourier coefficients are then functions of space, and under the assumptions of (1) negligible reflected waves, (2) slowly varying depth and (3) weak nonlinearity, first-order differential equations for the spatial evolution of the Fourier amplitudes can be derived. In this approach, the wave field in a physical domain can thus be found by integrating a set of first-order ordinary differential equations in one spatial sweep, taking refraction, shoaling and nonlinear interactions into account. If the phases of the Fourier amplitudes are retained in the modelling, the evolution equations are called deterministic. We shall focus on deterministic evolution equations in this paper. The models derived provide a numerically efficient tool for the description of shoaling, refraction and quadratic nonlinear interactions for wave fields in two horizontal dimensions.

Evolution equations are appropriate for describing nonlinear interactions between wave components. On an even depth quadratic interactions can be removed from the equations and evolution equations describing four-wave interactions (cubic nonlinearity) can be derived (see e.g. [1]). On variable depth, however, the quadratic interactions can be resonant in the form of class III Bragg resonance [2] and can thus not be eliminated. Further, in shallow water quadratic interactions can be nearly resonant, giving so-called triad interactions [3]. Contrary to four-wave interactions at deep water, triad interactions can build up over just a few wave lengths in shallow conditions and are thus important in coastal areas. Away from shallow and intermediate water, the quadratic interactions are non-resonant, giving rise to second-order bound waves, being phase locked to the first-order wave field. In this paper we shall retain only quadratic nonlinearity, thereby precluding any description of four-wave interactions. The models derived will provide a correct description of the second-order wave field from deep to shallow water, cubic effects being discarded.

Deterministic evolution equations have often been derived using a time domain Boussinesq formulation as starting point. Examples are Freilich and Guza [4], Liu, Yoon and Kirby [5], Yoon and Liu [6], Madsen and Sørensen [7], Chen and Liu [8] and Kaihatu and Kirby [9]. Boussinesq formulations make an attractive starting point, since they provide a depth-integrated formulation of the governing equations for water wave propagation. On the other hand, as Boussinesq formulations are derived as asymptotic expansions of the governing equations from the shallow water limit, their accuracy generally decays in deeper water.

As an alternative, evolution equations can be derived directly from the irrotational, inviscid governing equations. Hereby, the linear phase speed and shoaling characteristics agree exactly with linear wave theory for all depths. Such models are therefore denoted fully dispersive evolution equations. Agnon et al. [10] and Kaihatu and Kirby [11] derived fully dispersive evolution equations for the complex Fourier amplitudes of the still water potential. Both derivations involved depth-integration of the Laplace equation. Here the vertical variation of the velocity potential must be known a priori, and in both works the vertical structure of a linear wave was assumed. As a result, the second-order bound wave field is not modelled with exact amplitudes. Eldeberky and Madsen [12] pointed out that a quadratic transformation is needed, when results of the two above models are transformed from the still water potential to free surface elevations. Using this transformation, they derived evolution equations formulated directly in the complex Fourier amplitudes of the free surface elevation.

In this paper, a new derivation of fully dispersive deterministic evolution equations is given, free of assumptions on the vertical variation of the velocity potential. We hereby, for the first time, obtain models having exact second-order properties. We present evolution equations formulated in the complex Fourier amplitudes of either the still water potential or the free surface elevation. Both formulations are derived for an angular spectrum representation of the wave field, allowing for wave propagation in directions up to $\pm 90^\circ$ from the main direction of wave propagation. A weak deviation from straight and parallel depth contours is allowed for. By invoking the so-called 'resonance assumption' within the nonlinear terms, the models of Agnon et al. [10], Kaihatu and Kirby [11] and Eldeberky and Madsen [12] are recovered. Thus for short, we denote these models the 'resonant' models.

Having derived 'exact' as well as 'resonant' models, we analyse them with respect to second-order transfer functions for bichromatic wave propagation. The transfer functions derived are compared to the exact solution of a Stokes-type analysis of the governing equations as given by Sharma and Dean [13]. As expected the transfer of the 'exact' models is identical to the reference solution.

A well-known drawback of evolution equations is their representation of the nonlinear terms as convolution sums over the Fourier amplitudes. If a wave field contains N frequencies in time, the computational effort of evaluating these convolution sums is $\mathrm{O}(N^2)$. This has traditionally limited the use of evolution equations to wave fields with a relatively small number of frequencies. Recently, Bredmose, Schäffer and Madsen [14] have demonstrated that for the Boussinesq evolution equations of Madsen and Sørensen [7], the computational effort can be reduced to $\mathrm{O}(N \log N)$ by calculating the nonlinear terms with the aid of Fast Fourier Transforms. This technique, originally developed in the field of spectral methods for partial differential equations, is used here to improve the computational efficiency of the 'resonant' models. The FFT speed-up can also be applied to the angular spectrum variation, such that for N frequencies and M angular wave modes, the evolution equations can be solved at a cost of $\mathrm{O}((M\log M)(N\log N))$. This speed-up, however, is not applicable to the 'exact' models.

Although the 'exact' and 'resonant' models are derived for two-dimensional wave propagation, we here focus the validation on unidirectional waves. The models are applied to two cases of weakly nonlinear wave propagation over a submerged bar, using the experimental data of Beji and Battjes [15]. For a test of long waves ($kh = 0.32$ on the bar top), the second-order terms provide a clear improvement over results of linear theory, both with respect to wave shape and to release of higher harmonics as the waves leave the bar top. For a test of shorter waves ($kh = 0.68$ at the bar top), the wave shape on the bar top is improved as well by the second-order terms, but accumulative phase errors are observed, indicating an over-prediction of the amplitude dispersion in the models.

To look further into this, we extend the Stokes-type analysis of the models to third order, to obtain results for the amplitude dispersion and third-order transfer for unidirectional waves.

The structure of the paper is as follows. In Section 2, a review of fully dispersive evolution equations is given while in Section 3, the new exact models are derived. The bichromatic transfer functions for the new models are presented in Section 4 and the numerical speed-up technique using FFT is dealt with in Section 5. Model results for wave propagation over a submerged bar are presented in Section 6, and the third-order analysis in Section 7.

2. Review of fully dispersive evolution equations

2.1. The evolution equations of Agnon et al. [10]

The evolution equations of Agnon et al. [10] were formulated in the complex Fourier amplitudes of the still water potential and are valid for one horizontal dimension. The main steps in the derivation were the following: The free surface boundary conditions were expanded around the still water level and combined into a single equation in the still water potential. A multiple scales expansion in space and time was introduced to separate the fast and slow variation of the wave field. The governing equations were next transformed to Fourier space (with respect to time) and the Laplace equation depth-integrated. Initially, the vertical structure of bound waves as well as free waves was considered, that is

$$\phi(x,z,t) = \frac{\cosh k(z+h)}{\cosh kh}\phi(x,z=0,t) \tag{1}$$

where k can be a free wave number or a bound wave number. The model derived, however, was based on the vertical structure of a free wave. Agnon et al. [10] defined a detuning parameter

$$\mu = (k_{\mathrm{bound}} - k_{\mathrm{free}})/k_{\mathrm{free}} \tag{2}$$

giving a measure of the deviation between bound and free wave numbers. The bound waves within the model are thus described with an error of $\mathrm{O}(\mu)$.

The model was extended to two dimensions in Agnon and Sheremet [16], following the angular spectrum approach of Dalrymple and Kirby [17]. They also developed stochastic evolution equations based on the deterministic model, this topic, however, is not pursued in the present paper.

2.2. The evolution equations of Kaihatu and Kirby [11]

Kaihatu and Kirby [11] derived a set of evolution equations, essentially being an extension of the model of Agnon et al. [10] to weakly two-dimensional wave propagation. Their starting point was the Laplace equation, which was depth-integrated assuming a vertical structure of the velocity field corresponding to linear waves. The resulting equation was combined with the free surface conditions, giving a nonlinear mild-slope equation. Next the following expansion was utilised

$$\phi(x,y,t)|_{z=0} = \sum_{p=-N}^{N} -\frac{\mathrm{i}g}{\omega_p} a_p(x,y)\,\mathrm{e}^{\mathrm{i}(\int \bar{k}_p\,\mathrm{d}x - \omega_p t)}, \tag{3}$$

where y is the long-shore spatial coordinate and $\bar{k}_p$ is a y-averaged free wave number. The amplitudes $a_p(x,y)$ are complex numbers, satisfying $a_{-p} = a_p^*$ and $a_0 \in \mathbb{R}$. The frequencies are given as $\omega_p = p\omega_1$, where ω_1 is the smallest radian frequency resolved in the spectrum. As a next step, a slow variation of the Fourier amplitudes was assumed, that is $a_p = a_p(\delta^2 x, \delta y)$ where δ is a small ordering parameter. The resulting model thus only retained the derivatives $a_{p,x}$, $a_{p,y}$ and $a_{p,yy}$, thereby forming a set of evolution equations for a_p. Numerically, the y-dependence was allowed for by solving the equations on a set of parallel lines in the x-direction. The double y-derivative was then handled by a finite difference approximation. In an appendix, the model was extended to allow for a spatially varying current. For one horizontal dimension and no current, the model is identical to the model of Agnon et al. [10].

2.3. *The second-order transformation from ϕ to η*

Both of the two above models were compared to experimental results. Agnon et al. [10] simulated a laboratory test of almost unidirectional irregular waves propagating onto an open beach, and also field measurements of shoaling waves in Walker Bay, South Africa. Kaihatu and Kirby [11] simulated the test of Whalin [18] for regular wave propagation over a semicircular shoal and the test of breaking irregular waves on a plane sloping beach of Mase and Kirby [19]. For the latter purpose, the breaking model of Mase and Kirby [19] was incorporated.

In both of these works, however, the transformation between the Fourier amplitudes of the still water level and the Fourier amplitudes of the free surface elevation was linear. This is inconsistent with the second-order accuracy of the models, as pointed out by Eldeberky and Madsen [12]. Eldeberky and Madsen [12] gave a second-order transformation between these amplitudes and transformed the evolution equations of Agnon et al. [10], as well as Agnon and Sheremet [16], to sets of evolution equations formulated directly in the complex amplitudes of the free surface elevation. The correction of the transformation improves the accuracy of super-harmonic energy transfer significantly.

Kaihatu [20] discussed this correction of the deterministic model as well. The influence of the new second-order terms was examined by deriving fully nonlinear solutions to the equations in the amplitudes of the still water potential. The solutions were then transformed to free surface elevations, using either the linear transformation or the correct second-order transformation. In shallow water, essentially no difference was found, while at deep water, the effect was found to be more pronounced.

3. Derivation of the new evolution equations

In this section we present a new derivation of fully dispersive evolution equations, leading to a model with exact second-order transfer. We first derive a set of equations formulated in the complex Fourier amplitudes of the still water level potential. Subsequently, we transform these equations to the complex Fourier amplitudes of the free surface elevation.

3.1. *Governing equations and scaling*

We consider the motion of an inviscid irrotational fluid, as depicted in Fig. 1. A Cartesian coordinate system $(x, y, z) = (\mathbf{x}, z)$ with the z-axis pointing upwards from the still water level is adopted. The surface elevation is denoted $\eta(\mathbf{x}, t)$ and the velocity potential $\phi(\mathbf{x}, z, t)$. The velocity field within the fluid is (u, v, w) and g is the acceleration of gravity. The depth is described by $h(\mathbf{x})$, measuring the distance from the bottom to the still water level.

The governing equations are

$$\nabla^2\phi + \phi_{zz} = 0, \qquad -h < z < \eta, \tag{4}$$

$$\phi_z - \nabla\phi\cdot\nabla\eta - \eta_t = 0, \qquad z = \eta, \tag{5}$$

$$\phi_t + g\eta + \big((\nabla\phi)^2 + \phi_z^2\big)/2 = 0, \qquad z = \eta, \tag{6}$$

$$\phi_z + \nabla h\cdot\nabla\phi = 0, \qquad z = -h, \tag{7}$$

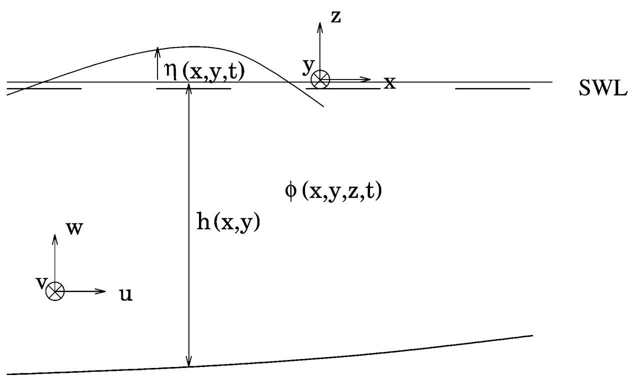

Fig. 1. Definition sketch for derivation of fully dispersive evolution equations.

stating local continuity (4), the kinematic and dynamic free surface conditions (5), (6), and impermeability of the bottom (7). $\boldsymbol{\nabla}$ is the horizontal gradient operator, i.e., $\boldsymbol{\nabla} = (\frac{\partial}{\partial x}, \frac{\partial}{\partial y})$. We shall assume a classical Stokes scaling of the variables, that is

$$\mathbf{x} = \frac{\mathbf{x}'}{k_0}, \qquad z = z'h_0, \qquad h = h'h_0,$$
$$t = \frac{t'}{\omega_0}, \qquad \eta = a_0\eta', \qquad \phi = \frac{ga_0}{\omega_0}\phi',$$

where a prime denotes dimensionless variables and $(k_0, h_0, \omega_0, a_0)$ are typical measures of wave number, depth, frequency and amplitude, respectively. This gives the nonlinearity parameter $\varepsilon = k_0 a_0$, which will appear as a factor on the nonlinear terms, if the above variables are inserted into the governing equations. However, instead of using the dimensionless variables, we shall carry out the derivation and analysis in the dimensional variables, keeping an artificial ε factor in front of the nonlinear terms. Thus in the following, ε is to be regarded as a small ordering parameter, which should simply be omitted in any numerical evaluation of the expressions. We thus assume weak nonlinearity of the wave field. Further, we assume that the sea bed is varying slowly as function of $\mathbf{x}$, i.e., $h = h(\varepsilon\mathbf{x})$, and that the deviation from uniform depth in the y-direction is $\mathrm{O}(\varepsilon)$.

3.2. Rewriting the governing equations

We follow the lines of Madsen and Schäeffer [21] and Agnon, Madsen and Schäffer [22], taking basis in an exact power series solution to the Laplace equation. The starting point is to expand the velocity potential as a power series in z:

$$\phi(\mathbf{x}, z, t) = \sum_{n=0}^{\infty} z^n \phi_n(\mathbf{x}, t). \tag{8}$$

It is easily seen that $\phi_0 = \phi(\mathbf{x}, 0, t) \equiv \Phi$ and $\phi_1 = w(\mathbf{x}, 0, t) \equiv W$. Further, insertion of (8) into the Laplace equation yields the well-known recursion relation $\phi_{n+2} = -\nabla^2\phi_n/((n+1)(n+2))$ and thereby the solution

$$\phi(\mathbf{x}, z, t) = \sum_{n=0}^{\infty} (-1)^n \frac{z^{2n}\nabla^{2n}}{(2n)!}\Phi + (-1)^n \frac{z^{2n+1}\nabla^{2n}}{(2n+1)!}W. \tag{9}$$

We identify the above series in $(z\boldsymbol{\nabla})$ as the Taylor series of the functions $\cos(z\nabla)$ and $\sin(z\nabla)/\nabla$, thus allowing us to write the series as

$$\phi(\mathbf{x}, z, t) = \mathrm{Cos}(z\nabla)\Phi + \frac{1}{\nabla}\mathrm{Sin}(z\nabla)W, \tag{10}$$

where the capitalised form of the trigonometric functions has been used to indicate that they denote operators. In the above equation both series operators are even functions of $\boldsymbol{\nabla}$. They are thus scalar operators, just like ∇^2. We indicate this by using a non-bold ∇ in their arguments and shall be using this convention throughout.

Next, we utilise the assumption of slowly varying depth, $h = h(\varepsilon\mathbf{x})$, and retain only first-order derivatives of the depth variation. As shown by Mei [23] and Agnon [24], a convenient way of dealing with this is to introduce a constant reference depth $h(\mathbf{x}) = h_0 + \delta(\mathbf{x})$ and expand the bottom boundary condition around h_0. This proves to be advantageous, when combining the sea bed condition with the series solution (10). We shall later resubstitute the true local depth h, and we thus note that the use of a reference level is just a technicality, that does not introduce any bounds on the depth range of model application. Taylor expanding the sea bed condition around the constant reference level h_0 yields

$$\phi_z + \delta\nabla^2\phi + \frac{1}{2}\delta^2\nabla^2\phi_z + \boldsymbol{\nabla}\delta\cdot(\boldsymbol{\nabla}\phi - \delta\boldsymbol{\nabla}\phi_z) = \mathrm{O}\big(\delta^3, \delta^2\boldsymbol{\nabla}\delta\big), \quad z = -h_0. \tag{11}$$

where the Laplace equation (4) has been used to rewrite double z-differentiations to ∇^2 operations. To lowest order, this equation states that $\phi_z = O(\delta, \boldsymbol{\nabla}\delta)$, allowing for writing the sea bed condition in the compact form

$$\phi_z = -\boldsymbol{\nabla}\cdot(\delta\boldsymbol{\nabla}\phi) + \mathrm{O}\big(\delta^3, \delta^2\boldsymbol{\nabla}\delta, \delta(\boldsymbol{\nabla}\delta)^2\big), \quad z = -h_0. \tag{12}$$

The advantage of this formulation is that it is defined on a constant level $z = -h_0$. All effects of varying depth are thus represented by δ and when the series solution (10) is inserted for ϕ, the operators will thus have the argument $h_0\boldsymbol{\nabla}$, where $\boldsymbol{\nabla}$ and h_0 can be interchanged. This simplifies the derivation considerably, since in general h and $\boldsymbol{\nabla}$ are not interchangeable. The assumption of mildly sloping bottom allows us to neglect all but first-order derivatives of δ, while as the last step in the derivation, we can replace the reference depth h_0 with the local depth h, implying $\delta = 0$ and $\boldsymbol{\nabla}\delta = \boldsymbol{\nabla}h$. Insertion of (10) into (12) yields

$$\mathrm{Sin}(h_0\nabla)\nabla\Phi + \mathrm{Cos}(h_0\nabla)W = -\boldsymbol{\nabla}\cdot\big\{\delta\big(\mathrm{Cos}(h_0\nabla)\boldsymbol{\nabla}\Phi - \mathrm{Sin}(h_0\nabla)W\big)\big\}. \tag{13}$$

We now invoke the free surface boundary conditions to express W in terms of Φ. Expanding (5) and (6) around $z=0$ yields

$$\eta_t - W + \varepsilon\big(\eta\nabla^2\Phi + \nabla\eta\cdot\nabla\Phi\big) = \mathrm{O}(\varepsilon^2) \tag{14}$$

$$g\eta + \phi_t + \varepsilon\big((\nabla\Phi)^2/2 + W^2/2 + \eta W_t\big) = \mathrm{O}(\varepsilon^2), \tag{15}$$

where we have used the Laplace equation to eliminate higher-order derivatives of Φ with respect to z. To lowest order, these equations read $W = \eta_t + \mathrm{O}(\varepsilon)$ and $\eta = -\Phi_t/g + \mathrm{O}(\varepsilon)$. This can be used to eliminate W and η in the nonlinear terms. We write the resulting equations as

$$-W - \frac{1}{g}\Phi_{tt} + \varepsilon\left[-\frac{1}{2g^3}\big(\Phi_t^2\big)_{ttt} + \frac{1}{2g^3}\big(\Phi_{tt}^2\big)_t - \frac{1}{g}\big((\nabla\Phi)^2\big)_t - \frac{1}{g}\Phi_t\nabla^2\Phi\right] = \mathrm{O}(\varepsilon^2), \tag{16}$$

$$g\eta + \Phi_t + \varepsilon\left[\frac{1}{2}(\nabla\Phi)^2 + \frac{1}{2g^2}\big(\Phi_t^2\big)_{tt} - \frac{1}{2g^2}\Phi_{tt}^2\right] = \mathrm{O}(\varepsilon^2). \tag{17}$$

3.3. Transforming to the frequency domain

Until now, the equations have been formulated in the time domain. We now transform them to the frequency domain, utilising the expansions

$$\eta(x,t) = \sum_{p=-N}^{N} \hat\eta_p(x,y)\,\mathrm{e}^{\mathrm{i}\omega_p t} = \sum_{p=-N}^{N}\sum_{l=-M}^{M} a_{p,l}(x)\,\mathrm{e}^{\mathrm{i}(\omega_p t - \int k_{p,l}^x\,\mathrm{d}x - k_l^y y)} \tag{18}$$

$$\Phi(x,t) = \sum_{p=-N}^{N} \hat\phi_p(x,y)\,\mathrm{e}^{\mathrm{i}\omega_p t} = \sum_{p=-N}^{N}\sum_{l=-M}^{M} b_{p,l}(x)\,\mathrm{e}^{\mathrm{i}(\omega_p t - \int k_{p,l}^x\,\mathrm{d}x - k_l^y y)}. \tag{19}$$

These expansions are Fourier series in time just like the expansion (3) with $\omega_p = p\omega_1$, $a_{-p,l} = a_{p,l}^*$, $a_{0,l}\in\mathbb{R}$ and similarly for $b_{p,l}$. As a difference to the expansion (3), we here treat the y-variation of the wave field through a Fourier expansion as well. This idea has been used by Dalrymple and Kirby [17], see also Dalrymple, Suh, Kirby and Chae [25], Suh, Dalrymple and Kirby [26], Chen and Liu [8] and Agnon and Sheremet [16], and makes it possible to treat waves propagating at angles deviating up to $\pm 90°$ from the x-direction. The wave numbers in the y-direction, k_l^y, are chosen with fixed increments, that is $k_l^y = lk_1^y$, where k_1^y is the smallest wave number resolved in the y-direction. For each frequency ω_p, and y-mode wave number k_l^y, the geometrical length of the wave number vector $\mathbf{k}_{p,l} = (k_{p,l}^x, k_l^y)$ is given by the linear dispersion relation. We denote this length by $k_p = |\mathbf{k}_{p,l}|$, and the x-component of $\mathbf{k}_{p,l}$ is then given by the Pythagorean relation

$$\big(k_{p,l}^x\big)^2 = k_p^2 - \big(k_l^y\big)^2. \tag{20}$$

Similarly to the above expansions, we expand W as

$$W(x,y) = \sum_{p=-N}^{N} \widehat{w}_p(x,y)\,\mathrm{e}^{\mathrm{i}\omega_p t}. \tag{21}$$

Substitution of this expansion and the first part of (19) into (16) then gives

$$\widehat{w}_p = \frac{\omega_p^2}{g}\hat\phi_p + \varepsilon\sum_{s=p-N}^{N} \mathrm{F}_{s,p-s}^{(2)}\hat\phi_s\hat\phi_{p-s} \tag{22}$$

with

$$\mathrm{F}_{s,p-s}^{(2)} = \frac{\mathrm{i}}{2g^3}\omega_s^2\omega_{p-s}^2\omega_p - \frac{\mathrm{i}}{2g^3}\omega_s\omega_{p-s}\omega_p^3 - \frac{\mathrm{i}}{g}\omega_p\boldsymbol{\nabla}_s\cdot\boldsymbol{\nabla}_{p-s} - \frac{\mathrm{i}}{2g}\omega_{p-s}(\nabla_s)^2 - \frac{1}{2g}\omega_s(\nabla_{p-s})^2, \tag{23}$$

where e.g. $\boldsymbol{\nabla}_s$ operates on ϕ_s only and similarly for $\boldsymbol{\nabla}_{p-s}$. We next transform the linear equation (13) to the frequency domain and insert the above result for $\widehat{w}_p$. This gives

$$\begin{aligned}&\mathrm{Sin}(h_0\nabla)\nabla\hat\phi_p + \mathrm{Cos}(h_0\nabla)\left[\frac{\omega_p^2}{g}\hat\phi_p + \varepsilon\sum_{s=p-N}^{N}\mathrm{F}^{(2)}\hat\phi_s\hat\phi_{p-s}\right]\\ &\quad = -\boldsymbol{\nabla}\cdot\left\{\delta\left(\mathrm{Cos}(h_0\nabla)\boldsymbol{\nabla}\hat\phi_p - \mathrm{Sin}(h_0\nabla)\frac{\omega_p^2}{g}\hat\phi_p\right)\right\} + \mathrm{O}(\varepsilon^2),\end{aligned} \tag{24}$$

where we have utilised that the right-hand side eventually becomes a bed-slope term of magnitude $\mathrm{O}(\varepsilon)$, such that the quadratic terms of $\widehat{w}_p$ can be consistently omitted here. Operation on both sides with the operator $\mathrm{Sec}(h_0\nabla)$ gives

$$\left(\nabla\,\mathrm{Tan}(h_0\nabla)+\frac{\omega_p^2}{g}\right)\hat{\phi}_p=-\,\mathrm{Sec}(h_0\nabla)\boldsymbol{\nabla}\cdot\left\{\delta\left(\mathrm{Cos}(h_0\nabla)\boldsymbol{\nabla}\hat{\phi}_p-\mathrm{Sin}(h_0\boldsymbol{\nabla})\frac{\omega_p^2}{g}\hat{\phi}_p\right)\right\}$$
$$-\,\varepsilon\sum_{s=p-N}^{N}\mathrm{F}^{(2)}_{s,p-s}\hat{\phi}_s\hat{\phi}_{p-s}+\mathrm{O}(\varepsilon^2). \tag{25}$$

3.4. Splitting the dispersion operator

For linear wave propagation on constant depth, the above equation states that

$$\left(\nabla\,\mathrm{Tan}(h_0\nabla)+\frac{\omega_p^2}{g}\right)\hat{\phi}_p=0 \tag{26}$$

and we denote the operator working on $\hat{\phi}$ in this expression as ‘the dispersion operator’. In the following we split this operator, to obtain a left-hand side appropriate for evolution equations. We follow the lines of Agnon [24], who split the dispersion operator to obtain a mild-slope equation.

The Tan-operator is to be interpreted through its infinite Taylor series, and the operator as a whole can therefore be considered as a polynomial in $\boldsymbol{\nabla}$ of infinite order. Two of the roots are the progressive linear wave numbers $\boldsymbol{\nabla}=\pm\mathrm{i}\mathbf{k}_p$. This can be seen by insertion, using that $\tan(\mathrm{i}u)=\mathrm{i}\tanh u$. As the operator is even in $\mathbf{k}_p$, one obtains the scalar result $-k_p\tanh k_ph_0+\omega_p^2/g=0$, the well known dispersion relation for linear water waves. Besides the progressive wave number solutions, there is an infinite set of evanescent wave modes, represented by the roots $\boldsymbol{\nabla}=(\pm\mathbf{k}_1^{\mathrm{ev}},\pm\mathbf{k}_2^{\mathrm{ev}},\ldots)$. The polynomial can be factorised, with each of the factors being $(\boldsymbol{\nabla}-\boldsymbol{\nabla}_{\mathrm{root}})$. One of these factors is $(\boldsymbol{\nabla}+\mathrm{i}\mathbf{k}_p)$, and we define the remaining factor by

$$\left(\nabla\,\mathrm{Tan}(h_0\nabla)+\frac{\omega_p^2}{g}\right)\equiv\frac{\boldsymbol{\nabla}+\mathrm{i}\mathbf{k}_p}{\mathrm{H}(h_0\boldsymbol{\nabla},\mathbf{k}_ph_0)} \tag{27}$$

which implies

$$\mathrm{H}(h_0\boldsymbol{\nabla},\mathbf{k}_ph_0)=\frac{h_0\boldsymbol{\nabla}+\mathrm{i}\mathbf{k}_ph_0}{h_0\nabla\,\mathrm{Tan}(h_0\nabla)+k_ph_0\tanh k_ph_0}. \tag{28}$$

We now apply the above result to (25) to obtain

$$(\boldsymbol{\nabla}+\mathrm{i}\mathbf{k}_p)\hat{\phi}_p=-\mathrm{H}(h_0\boldsymbol{\nabla},\mathbf{k}_ph_0)\,\mathrm{Sec}(h_0\nabla)\boldsymbol{\nabla}\cdot\left\{\delta\left(\mathrm{Cos}(h_0\nabla)\boldsymbol{\nabla}\hat{\phi}_p-\mathrm{Sin}(h_0\boldsymbol{\nabla})\frac{\omega_p^2}{g}\hat{\phi}_p\right)\right\}$$
$$-\,\varepsilon\sum_{s=p-N}^{N}\mathrm{H}(h_0\boldsymbol{\nabla},\mathbf{k}_ph_0)\mathrm{F}^{(2)}_{s,p-s}\hat{\phi}_s\hat{\phi}_{p-s}. \tag{29}$$

This is a set of evolution equations in the Fourier amplitudes of the still water potential. In the following, we express the infinite series operators involved in terms of free wave numbers, thus turning the above equation into a practically applicable model.

We first treat the bed slope term (the one involving δ). Using (26) we write this as

$$T_{\mathrm{bed}}=-\frac{\mathrm{Sec}(h_0\nabla)}{h_0\nabla\mathrm{Tan}(h_0\nabla)+k_ph_0\tanh(k_ph_0)}(h_0\boldsymbol{\nabla}+\mathrm{i}\mathbf{k}_ph_0)\boldsymbol{\nabla}\cdot\left\{\delta\,\mathrm{Sec}(h_0\nabla)\boldsymbol{\nabla}\hat{\phi}_p\right\}. \tag{30}$$

To discard all but first-order derivatives of δ, we insert

$$\boldsymbol{\nabla}=\boldsymbol{\nabla}^{\mathrm{w}}+\boldsymbol{\nabla}^{\delta} \tag{31}$$

where it is understood that $\boldsymbol{\nabla}^{\delta}$ operates solely on δ, while $\boldsymbol{\nabla}^{\mathrm{w}}$ operates solely on ϕ. We next Taylor expand in $\boldsymbol{\nabla}^{\delta}$ and retain only the first-order term in $\boldsymbol{\nabla}^{\delta}$. For doing this we rewrite (30) to a scalar expression. The first operator in (30) (the fraction) is scalar, and thus just a function of the scalar argument

$$r=\sqrt{\boldsymbol{\nabla}\cdot\boldsymbol{\nabla}}=\sqrt{\left(\nabla^{\mathrm{w}}\right)^2+2\boldsymbol{\nabla}^{\mathrm{w}}\cdot\boldsymbol{\nabla}^{\delta}+\left(\nabla^{\delta}\right)^2}. \tag{32}$$

Further, as to lowest order $\nabla^{\mathrm{w}} = -\mathrm{i}\mathbf{k}_p$, the remaining part of T_{bed} can be written $h_0\nabla^\delta(\nabla^{\mathrm{w}} + \nabla^\delta)\cdot(\delta\,\mathrm{Sec}(h_0\nabla^{\mathrm{w}})\nabla^{\mathrm{w}}\hat{\phi}_p)$ and thus

$$T_{\text{bed}} = -\frac{\mathrm{Sec}(h_0 r)\,\mathrm{Sec}(h_0\nabla^{\mathrm{w}})}{r\,\mathrm{Tan}(h_0 r) + k_p\tanh(k_p h_0)}\nabla^\delta\big((\nabla^{\mathrm{w}})^2 + \nabla^\delta\cdot\nabla^{\mathrm{w}}\big)\delta\hat{\phi}_p. \tag{33}$$

As we have assumed that the lateral variation of h is weak, we can use $\nabla^\delta = (\partial_x^\delta, 0)$ in the above term, where ∂_x^δ is operating solely on δ. Thereby only the first vectorial component is non-zero, and we can express this as

$$\widetilde{T}_{\text{bed}} = -\frac{\mathrm{Sec}(h_0\tilde{r})\,\mathrm{Sec}(h_0\nabla^{\mathrm{w}})}{\tilde{r}\,\mathrm{Tan}(h_0\tilde{r}) + k_p\tanh k_p h}\partial_x^\delta\big((\nabla^{\mathrm{w}})^2 + \partial_x^\delta\partial_x^w\big)\delta\hat{\phi} \tag{34}$$

with $\tilde{r} = \sqrt{(\nabla^{\mathrm{w}})^2 - 2\mathrm{i}k_p^x\partial_x^\delta + (\partial_x^\delta)^2}$ and where k_p^x is the x-component of the wave number vector. The right-hand side in (34) is a scalar operator that can easily be expanded around $\partial_x^\delta = 0$. Schematically, the result is

$$\widetilde{T}_{\text{bed}} = \mathrm{OP}_1\delta\hat{\phi}_p + \mathrm{OP}_2\delta_x\hat{\phi}_p + \mathrm{OP}_3\delta_{xx}\hat{\phi}_p + \cdots \tag{35}$$

and we truncate after the δ_x term, as we have assumed a mild slope of the sea bed. Further, we shall after the expansion set the reference level h_0 equal to the local depth h, implying $h_0 = h(\mathbf{x})$ and thus $\delta = 0$, $\delta_x = h_x$. In this process the first term in the above expansion vanishes, and we are left with the second term which upon insertion of $\nabla^{\mathrm{w}} = -\mathrm{i}\mathbf{k}_p$ can be evaluated to

$$\widetilde{T}_{\text{bed}} = \kappa\frac{\kappa^2(2\kappa + 2\sinh(2\kappa)) + (k_p^x h)^2(2\kappa\cosh(2\kappa) - 3\sinh(2\kappa) - 4\kappa)}{(k_p^x h)^2(2\kappa + \sinh(2\kappa))^2}\frac{h_x}{h}\hat{\phi}_p = -\frac{1}{2c_{gp}^x}\frac{\partial}{\partial x}\{c_{gp}^x\}\hat{\phi}_p \tag{36}$$

where $\kappa = k_p h$ and c_{gp}^x is the x-component of the group velocity vector $\frac{\partial\omega_p}{\partial k_p}\frac{\mathbf{k}_p}{k_p}$. The latter form of the bed slope term is well established in the literature, see e.g. Radder [27], Dalrymple and Kirby [17] and Agnon and Sheremet [16]. We emphasise that no bounds on the depth variation applies for this term, except for the mild slope assumption. Defining $\nabla_x = (\frac{\partial}{\partial x}, 0)$, we can incorporate the above result into (29) in the following way

$$(\nabla + \mathrm{i}\mathbf{k}_p)\hat{\phi}_p = -\varepsilon\frac{\nabla_x\{c_{gp}^x\}}{2c_{gp}^x}\hat{\phi}_p - \varepsilon\sum_{s=p-N}^{N}\mathrm{H}(h\nabla, k_p h)\mathrm{F}^{(2)}_{s,p-s}\hat{\phi}_s\hat{\phi}_{p-s}. \tag{37}$$

3.5. Expanding in the y-direction

We now expand this result in the y-direction. Following Dalrymple et al. [25], we allow for a weak deviation from straight and parallel bottom contours by defining a set of laterally averaged wave numbers

$$\bar{k}_p^2(x) = \frac{1}{L_y}\int_0^{L_y} k_p^2(x,y)\,\mathrm{d}y; \qquad \frac{k_p^2(x,y)}{\bar{k}_p^2(x)} = 1 - \nu_p(x,y) \tag{38}$$

where we assume $\nu_p \leqslant \mathrm{O}(\varepsilon)$. Similarly, we define a set of x-wave numbers

$$\big(\bar{k}_{p,l}^x(x)\big)^2 = \bar{k}_p^2 - \big(k_l^y\big)^2. \tag{39}$$

Due to the assumption $\nu_p \leqslant \mathrm{O}(\varepsilon)$ we can use the laterally averaged wave numbers in all terms on the right-hand side of (37), the error being $\mathrm{O}(\varepsilon^2)$. We thus insert the right-most part of the expansion (19) using the laterally averaged wave numbers into (37). As the Fourier amplitudes $b_{p,l}$ are independent of y, we are only interested in the first coordinate of the resulting equation, describing the variation in the x-direction. This reads

$$\sum_{l=-M}^{M}\left\{\frac{\partial b_{p,l}}{\partial x} + \mathrm{i}\big(k_{p,l}^x - \bar{k}_{p,l}^x\big)b_{p,l}\right\}\mathrm{e}^{-\mathrm{i}(\int\bar{k}_{p,l}^x\,\mathrm{d}x + k_l^y y)} = -\varepsilon\frac{1}{2c_{gp}^x}\frac{\partial c_{gp}^x}{\partial x}\hat{\phi}_p - \varepsilon\sum_{s=p-N}^{N}\widetilde{\mathrm{H}}(h\nabla, k_p h)\mathrm{F}^{(2)}_{s,p-s}\hat{\phi}_s\hat{\phi}_{p-s}, \tag{40}$$

where the right-hand side has been written in its unexpanded form for simplicity and $\widetilde{\mathrm{H}}$ denotes the first vectorial component of H, see (46).

The above equation is not easily decoupled into separate equations for $\partial b_{p,l}/\partial x$, since $k^x_{p,l}$ depends on y as well as l. Following Dalrymple et al. [25] we get around this by observing that subtracting (39) from (20) gives $k_p^2 - \bar{k}_p^2 = 2\bar{k}^x_{p,l}(k^x_{p,l} - \bar{k}^x_{p,l}) + \mathrm{O}(\nu_p^2)$ and thus by invoking (38)

$$k^x_{p,l} - \bar{k}^x_{p,l} = -\frac{\bar{k}_p^2}{2\bar{k}^x_{p,l}}\nu_p + \mathrm{O}\big(\nu_p^2\big). \tag{41}$$

Insertion of this into (40) gives

$$\sum_{l=-M}^{M}\left\{\frac{\partial b_{p,l}}{\partial x} - \mathrm{i}\frac{\bar{k}_p^2}{2\bar{k}^x_{p,l}}\nu_p b_{p,l}\right\}\mathrm{e}^{-\mathrm{i}(\int \bar{k}^x_{p,l}\,\mathrm{d}x + k^y_l y)} = -\varepsilon\frac{1}{2c^x_{gp}}\frac{\partial c^x_{gp}}{\partial x}\hat{\phi}_p - \varepsilon\sum_{s=p-N}^{N}\widetilde{\mathrm{H}}(h\nabla, k_p h)\mathrm{F}^{(2)}_{s,p-s}\hat{\phi}_s\hat{\phi}_{p-s}, \tag{42}$$

which is easily decoupled using the lateral Fourier expansion of ν_p

$$\nu_p = \sum_{l=-M}^{M}\hat{\nu}_{p,l}\,\mathrm{e}^{-\mathrm{i}k^y_l y}. \tag{43}$$

The product of ν_p and $b_{p,l}$ can thus be expressed through a convolution in the same way as in the nonlinear terms. This produces the model

$$\begin{aligned}\frac{\partial b_{p,l}}{\partial x} = {}& -\varepsilon\frac{1}{2c^x_{gp}}\frac{\partial c^x_{gp}}{\partial x}b_{p,l} + \varepsilon\mathrm{i}\frac{\bar{k}_p^2}{2\bar{k}^x_{p,l}}\sum_{t=\max\{l-M,-M\}}^{\min\{l+M,M\}}\hat{\nu}_{p,t}b_{p,l-t}\\ & - \varepsilon\sum_{s=p-N}^{N}\sum_{t=\max\{l-M,-M\}}^{\min\{l+M,M\}}\widetilde{\mathrm{H}}(h\nabla, \bar{\mathbf{k}}_{p,l}h)\widetilde{\mathrm{F}}^{(2)}_{s,p-s,t,l-t}b_{s,t}b_{p-s,l-t}\,\mathrm{e}^{-\mathrm{i}\int(\bar{k}^x_{s,t} + \bar{k}^x_{p-s,l-t} - \bar{k}^x_{p,l})\,\mathrm{d}x},\end{aligned} \tag{44}$$

where

$$\widetilde{\mathrm{F}}^{(2)}_{s,p-s,t,l-t} = \frac{\mathrm{i}}{2g^3}\omega_s^2\omega_{p-s}^2\omega_p - \frac{\mathrm{i}}{2g^3}\omega_s\omega_{p-s}\omega_p^3 + \frac{\mathrm{i}}{g}\omega_p\bar{\mathbf{k}}_{s,t}\cdot\bar{\mathbf{k}}_{p-s,l-t} + \frac{\mathrm{i}}{2g}\omega_{p-s}k_s^2 + \frac{\mathrm{i}}{2g}\omega_s k_{p-s}^2 \tag{45}$$

and

$$\widetilde{\mathrm{H}}(h\nabla, \mathbf{k}_{p,l}h) = \frac{h_0\partial_x + \mathrm{i}k^x_{p,l}h}{h\nabla\,\mathrm{Tan}(h\nabla) + k_p h\tanh k_p h}. \tag{46}$$

This is the main result of this paper, along with a similar set of evolution equations formulated in the wave amplitudes for the free surface elevation η, see (53). In the summation range for the outer sum of (44) we have assumed that p is always positive. This is due to the requirement $b_{-p,l} = b^*_{p,l}$ ensuring that the time series for ϕ is real and eliminating the need for solving for negative values of p. A similar symmetry, however, does not apply for the l-index, and the summation ranges must therefore allow for positive as well as negative values of l. In this context it should be noted that the summation ranges can be reduced further, utilising symmetry properties of the summation. However, as we find the above notation easier to work with, we do not go further into this. Details on such reductions can be found in e.g., Mei [28].

The above model describes the transformation of a directionally spread wave field over slowly varying bathymetry, including second-order nonlinearity. Depth changes in the x-direction implies changes of amplitude (the first term on the right-hand side) as well as phase changes (through change of $\bar{k}^x_{p,l}$ in the exponential functions), while depth changes in the y-direction only gives rise to phase changes (second term on the right-hand side).

3.6. The 'resonant' and 'exact' model

In the above result, (44), we have not yet inserted an expression for ∇ in the H-operator within the nonlinear terms. For each pair of interacting wave components, we may approximate the gradient of their product by the values associated with their linear wave numbers. This corresponds to setting $\nabla = -\mathrm{i}(\mathbf{k}_{s,t} + \mathbf{k}_{p-s,l-t})$ in each term of the sum. This results in a model which has exact second-order transfer functions.

Another approach is to assume resonance of the forcing nonlinear terms with the free wave mode at the receiving frequency. This amounts to assuming $\nabla = -\mathrm{i}\mathbf{k}_{p,l}$. Doing so, the model of Agnon and Sheremet [16] is recovered, agreeing for the unidirectional case with the model of Kaihatu and Kirby [11]. The resonance assumption is only valid in shallow water, where the dispersion is vanishing.

We note that $\widetilde{\mathrm{H}}(h\nabla, \mathbf{k}_{p,l}h)$ is not singular for $\nabla = -\mathrm{i}\mathbf{k}_{p,l}$. To evaluate its value at resonance, we consider the limit for $\nabla = (\partial_x, -\mathrm{i}k_l^y) \to -\mathrm{i}\mathbf{k}_{p,l}$, i.e. the limit for fixed y-wave number. We obtain

$$\begin{aligned}\lim_{\nabla\to\mathbf{k}_{p,l}} \widetilde{\mathrm{H}}(h\nabla, \mathbf{k}_{p,l}h) &= \lim_{k'^x \to k^x_{p,l}} \frac{-\mathrm{i}k^{x'} + \mathrm{i}k^x_{p,l}}{-\omega'^2/g + \omega_p^2/g} \\ &= \lim_{k'\to k} \mathrm{i}g \frac{1}{\cos\theta_{p,l}} \frac{k' - k_p}{\omega'^2 - \omega_p^2} = \frac{\mathrm{i}g}{\cos\theta_{p,l}} \frac{\partial k_p}{\partial \omega_p^2} = \frac{\mathrm{i}g}{2\omega_p c_{gp} \cos\theta_{p,l}},\end{aligned} \tag{47}$$

where $\omega'^2 = gk' \tanh k'h$ and $\theta_{p,l}$ is the angle between the x-direction and the wave number vector $\mathbf{k}_{p,l}$. We look closer at the two different interaction kernels ('exact', 'resonant') in Sections 4 and 7.

3.7. Evolution equations in η

The evolution equations (37) can be transformed into evolution equations in the complex amplitudes of the free surface elevation, η. Such a transformation was presented by Eldeberky and Madsen [12] for the models of Agnon et al. [10] and Kaihatu and Kirby [11]. We follow the same route here.

A second-order relation between $\hat{\eta}_p$ and $\hat{\phi}_p$ can be derived by inserting the expansions (18)–(19) into the dynamic free surface boundary condition (17). To lowest order the resulting equation reads $\hat{\phi}_p = (\mathrm{i}g/\omega_p)\hat{\eta}_p + \mathrm{O}(\varepsilon)$, which can be used in the quadratic terms within the second-order accuracy. We hereby obtain the relation

$$\hat{\phi}_p = \frac{\mathrm{i}g}{\omega_p}\hat{\eta}_p + \varepsilon\mathrm{i}\sum_{s=p-N}^{N} \mathrm{T}^{(2)}_{s,p-s}\hat{\eta}_s\hat{\eta}_{p-s} + \mathrm{O}(\varepsilon^2), \tag{48}$$

$$\mathrm{T}^{(2)}_{s,p-s} = \frac{g^2}{2\omega_p\omega_s\omega_{p-s}}\mathbf{k}_s\cdot\mathbf{k}_{p-s} - \frac{1}{2}\omega_p + \frac{\omega_s\omega_{p-s}}{2\omega_p}. \tag{49}$$

We now calculate $(\nabla + \mathrm{i}\mathbf{k}_p)\hat{\phi}_p$ from this expression. For each of the nonlinear terms in the summation of (48), we use the linear approximation $(\nabla + \mathrm{i}\mathbf{k}_p) = (-\mathrm{i}(\mathbf{k}_s + \mathbf{k}_{p-s}) + \mathrm{i}\mathbf{k}_p)$ to obtain

$$(\nabla + \mathrm{i}\mathbf{k}_p)\hat{\phi}_p = \frac{\mathrm{i}g}{\omega_p}(\nabla + \mathrm{i}\mathbf{k}_p)\hat{\eta}_p + \varepsilon\sum_{s=p-N}^{N}(\mathbf{k}_s + \mathbf{k}_{p-s} - \mathbf{k}_p)\mathrm{T}^{(2)}_{s,p-s}\hat{\eta}_s\hat{\eta}_{p-s}. \tag{50}$$

In (37) we can easily express the quadratic products in terms of the $\hat{\eta}$ amplitudes, again using the linear part of (48). Combining the resulting equation with the above expression yields

$$(\nabla + \mathrm{i}\mathbf{k}_p)\hat{\eta}_p = -\varepsilon\frac{\nabla_x\{c^x_{gp}\}}{2c^x_{gp}}\hat{\eta}_p + \mathrm{i}\varepsilon\sum_{s=p-N}^{N}\mathrm{W}_{s,p-s}\hat{\eta}_s\hat{\eta}_{p-s} \tag{51}$$

with

$$\mathrm{W}_{s,p-s} = \frac{\omega_p}{g}(\mathbf{k}_s + \mathbf{k}_{p-s} - \mathbf{k}_p)\mathrm{T}^{(2)}_{s,p-s} - g\frac{\omega_p}{\omega_s\omega_{p-s}}\mathrm{H}(h\nabla, \mathbf{k}_p h)\mathrm{F}^{(2)}_{s,p-s}, \tag{52}$$

where $\mathrm{T}^{(2)}_{s,p-s}$, $\mathrm{F}^{(2)}_{s,p-s}$ and $\mathrm{H}(h\nabla, \mathbf{k}_p h)$ are defined in (48), (23) and (28), respectively.

When the y-dependence of the wave amplitudes is treated through a Fourier expansion, corresponding to the right-most expansion in (18), the resulting model reads

$$\begin{aligned}\frac{\partial a_{p,l}}{\partial x} &= -\varepsilon\frac{1}{2c^x_{gp}}\frac{\partial c^x_{gp}}{\partial x}a_{p,l} + \varepsilon\mathrm{i}\frac{\bar{k}_p^2}{2\bar{k}^x_{p,l}}\sum_{t=\max\{l-M,-M\}}^{\min\{l+M,M\}}\hat{\nu}_{p,t}a_{p,l-t} \\ &\quad + \mathrm{i}\varepsilon\sum_{s=p-N}^{N}\sum_{t=\max\{l-M,-M\}}^{\min\{l+M,M\}}\widetilde{\mathrm{W}}_{s,p-s,t,l-t}a_{s,t}a_{p-s,l-t}\,\mathrm{e}^{-\mathrm{i}\int(\bar{k}^x_{s,t} + \bar{k}^x_{p-s,l-t} - \bar{k}^x_{p,l})\,\mathrm{d}x}\end{aligned} \tag{53}$$

with

$$\widetilde{\mathrm{W}}_{s,t,p-s,l-t} = \left(\bar{k}^x_{s,t} + \bar{k}^x_{p-s,l-t} - \bar{k}^x_{p,l}\right)\left(\frac{g}{2\omega_s\omega_{p-s}}\bar{\mathbf{k}}_{s,t}\cdot\bar{\mathbf{k}}_{p-s,l-t} - \frac{\omega_p^2}{2g} + \frac{\omega_s\omega_{p-s}}{2g}\right) - g\frac{\omega_p}{\omega_s\omega_{p-s}}\widetilde{\mathrm{H}}(h\boldsymbol{\nabla}, \bar{\mathbf{k}}_{p,l}h)\widetilde{\mathrm{F}}^{(2)}_{s,t,p-s,l-t}. \quad (54)$$

For no y-dependence of the bathymetry, use of the resonance assumption $\boldsymbol{\nabla} = -\mathrm{i}\mathbf{k}_{p,l}$ in the $\widetilde{\mathrm{H}}$-term recovers the model of Eldeberky and Madsen [12], while use of the linear approximation, $\boldsymbol{\nabla} = -\mathrm{i}(\mathbf{k}_s + \mathbf{k}_{p-s})$, yields a model with exact second-order transfer for bichromatic waves. This particular model forms the main result of this paper together with (44). As already mentioned, the above equations describe the evolution of a complex directional wave spectrum due to varying depth and nonlinear interactions in terms of a set of coupled ordinary differential equations.

4. Second-order bichromatic transfer functions

We now analyse the evolution equations derived with respect to second-order bichromatic transfer functions. The reference solution can be obtained by applying a Stokes expansion technique to the governing equations (4)–(7) and deriving the amplitudes of the second-order bound wave field given the amplitudes of the first-order primary wave field.

We here cite the solution of Sharma and Dean [13], but using the notation of Schäffer and Steenberg [29]. For a primary progressive wave field on constant depth of the form

$$\eta^{(1)} = \frac{1}{2}A_n\,\mathrm{e}^{\mathrm{i}\theta_n} + \frac{1}{2}A_m\,\mathrm{e}^{\mathrm{i}\theta_m} + \text{c.c.}, \quad \theta_j = \omega_j t - \mathbf{k}_j\cdot\mathbf{x}, \quad (55)$$

with $\mathbf{k}_n \neq \mathbf{k}_m$, the second-order bound wave field is

$$\eta^{(2)} = \frac{1}{2}G_{n,m}A_nA_m\,\mathrm{e}^{\mathrm{i}(\theta_n+\theta_m)} + \frac{1}{2}G_{n,n}A_nA_n\mathrm{e}^{2\mathrm{i}\theta_n} + \frac{1}{2}G_{m,m}A_mA_m\,\mathrm{e}^{2\mathrm{i}\theta_m} + \frac{1}{2}G_{n,-m}A_nA_{-m}\,\mathrm{e}^{\mathrm{i}(\theta_n-\theta_m)} + \text{c.c.} \quad (56)$$

where

$$G_{n,m} = \frac{\tilde{\delta}_{n,m}}{g}\left((\omega_n+\omega_m)\frac{H_{n,m}}{D_{n,m}} - L_{n,m}\right), \quad (57)$$

$$\tilde{\delta}_{n,m} = \begin{cases} \frac{1}{2} & \text{for } \mathbf{k}_n = \mathbf{k}_m, \\ 1, & \text{otherwise,} \end{cases} \quad (58)$$

$$H_{n,m} = (\omega_n+\omega_m)\left(\omega_n\omega_m - \frac{g^2\mathbf{k}_n\cdot\mathbf{k}_m}{\omega_n\omega_m}\right) + \frac{1}{2}\left(\omega_n^3+\omega_m^3\right) - \frac{g^2}{2}\left(\frac{k_n^2}{\omega_n} + \frac{k_m^2}{\omega_m}\right), \quad (59)$$

$$D_{n,m} = gK_{nm}\tanh K_{nm}h - (\omega_n+\omega_m)^2, \quad (60)$$

$$K_{nm} = |\mathbf{k}_n + \mathbf{k}_m|, \quad (61)$$

$$L_{n,m} = \frac{1}{2}\left(\frac{g^2\mathbf{k}_n\cdot\mathbf{k}_m}{\omega_n\omega_m} - \omega_n\omega_m - \left(\omega_n^2+\omega_m^2\right)\right). \quad (62)$$

In the above notation, the convention $A_{-j} = A_j^*$, $\omega_{-j} = -\omega_j$, $\mathbf{k}_{-j} = -\mathbf{k}_j$ is used. This eliminates the need for distinguishing between sub-harmonic and super-harmonic bound waves. Super-harmonic waves are obtained by taking both n and m positive, while sub-harmonic waves are obtained by taking n positive and m negative.

We now derive the transfer function $G_{n,m}$ for evolution equations. For two primary wave components

$$\eta^{(1)} = a_n\,\mathrm{e}^{\mathrm{i}(\omega_n t - \mathbf{k}_n\cdot x)} + a_m\,\mathrm{e}^{\mathrm{i}(\omega_m t - \mathbf{k}_m\cdot x)} + \text{c.c.} \quad (63)$$

with $\mathbf{k}_n \neq \mathbf{k}_m$, four bound wave components, $\eta^{(2)}_{n,m}$, $\eta^{(2)}_{n,n}$, $\eta^{(2)}_{m,m}$, $\eta^{(2)}_{n,-m}$ will be forced. Their evolution will be described with one equation for each, which can be expressed as

$$\frac{\partial a_{r+q,r+q}}{\partial x} = 2\mathrm{i}\tilde{\delta}_{r,q}\widetilde{\mathrm{W}}_{r,q}a_ra_q\,\mathrm{e}^{-\mathrm{i}(k_r^x+k_q^x-k^x_{r+q,r+q})x}, \quad (64)$$

where (r,q) can take the values (n,m), (n,n), (m,m) and $(n,-m)$ and the usual four indices of $\widetilde{\mathrm{W}}$ have been replaced by the two indices (r,q) similarly to the adopted one-index notation for the forcing waves (a_n, a_m). Integration with respect to x gives

$$a_{r+q,r+q} = -\frac{2\tilde{\delta}_{r,q}\widetilde{\mathrm{W}}_{r,q}a_ra_q}{k_r^x + k_q^x - k^x_{r+q,r+q}}\,\mathrm{e}^{-\mathrm{i}(k_r^x+k_q^x-k^x_{r+q,r+q})x}. \quad (65)$$

Matching (63) with (55) gives $a_r = \frac{1}{2}A_r$ and similar for q, and the physical wave field of the above bound wave component is thus

$$\eta_{\text{bound}} = -\frac{1}{2}\frac{\tilde{\delta}_{r,q}\widetilde{\mathrm{W}}_{r,q}A_r A_q}{k_r^x + k_q^x - k_{r+q,r+q}^x}\,\mathrm{e}^{\mathrm{i}((\omega_r+\omega_q)t-(k_r^x+k_q^x)x-(k_r^y+k_q^y)y)} + \text{c.c.} \tag{66}$$

which corresponds to the first component in (56) for $(r,q) = (n,m)$, the second for $(r,q) = (n,n)$ and the third and fourth for $(r,q) = (m,m), (n,-m)$, respectively. Matching these expressions thus establishes the result for the bichromatic transfer function of the evolution equations

$$G_{n,m}^{\text{Evo}} = -\frac{\tilde{\delta}_{n,m}\widetilde{\mathrm{W}}_{n,m}}{k_n^x + k_m^x - k_{n+m,n+m}^x}. \tag{67}$$

Given a kernel $\widetilde{\mathrm{W}}_{n,m}$ for a set of evolution equations, their second-order bichromatic transfer functions can thus be determined and compared to the target solution (57)–(62). We note that since (44) and (53) are consistent to second order, these models have identical second-order properties.

4.1. Comparison of transfer functions

As a first check, the transfer functions of the 'exact' evolution equations were compared analytically to the transfer functions (57). This was done using Mathematica, and it was found that the transfer functions are identical. This agreement of the exact second-order transfer functions is the test proving that the models (44) and (53) are consistent second-order models, when $\boldsymbol{\nabla} = -\mathrm{i}(\mathbf{k}_s + \mathbf{k}_{p-s})$ is inserted into the kernel function.

We next turn to the 'resonant' models. As an analytical check, the kernel function $\mathrm{W}_{s,p-s}$ of (53) with $\boldsymbol{\nabla} = -\mathrm{i}\mathbf{k}_{p,l}$ was compared to the kernel of the equations of Eldeberky and Madsen [12], again with the aid of Mathematica, yielding a perfect match.

Next, we compare the transfer functions of the 'resonant' model to the exact transfer functions. We here focus on unidirectional wave propagation. In Fig. 2, G_{11}^{Evo}, the transfer function for self-self interaction, is plotted against dimensionless angular frequency $\omega(h/g)^{1/2}$ for the 'resonant' model. The result is normalised with the exact transfer function (57). The transfer function is remarkably close to the reference solution, the largest deviation being an over-prediction of 3.5% at intermediate depth. The full range of bichromatic transfer, still for unidirectional wave propagation is examined in Fig. 3, where the ratio between $G_{n,m}^{\text{Evo}}$ and $G_{n,m}^{\text{Stokes}}$ is plotted for $(\omega_n(h/g)^{1/2}, \omega_m(h/g)^{1/2}) \in [0; 2\pi]^2$. The super harmonic transfer of the evolution equations is very close to the target of Stokes theory. The small variation observed for the self-self interaction is seen as two small curves close to the diagonal. The reason for the good agreement in the super-harmonic region is that $\widetilde{\mathrm{F}}_{s,p-s}^{(2)}$ decays to zero

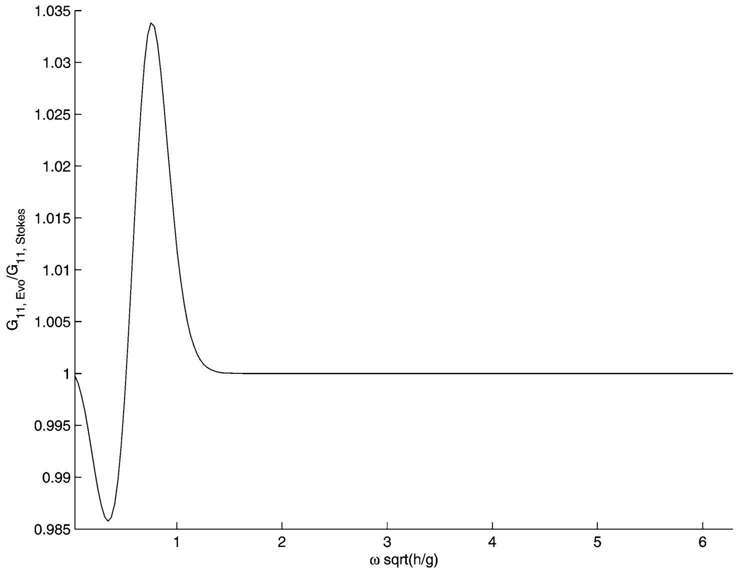

Fig. 2. Second-order self-self interaction transfer function for evolution equations invoking the resonance assumption. The values are normalised with the exact transfer function.

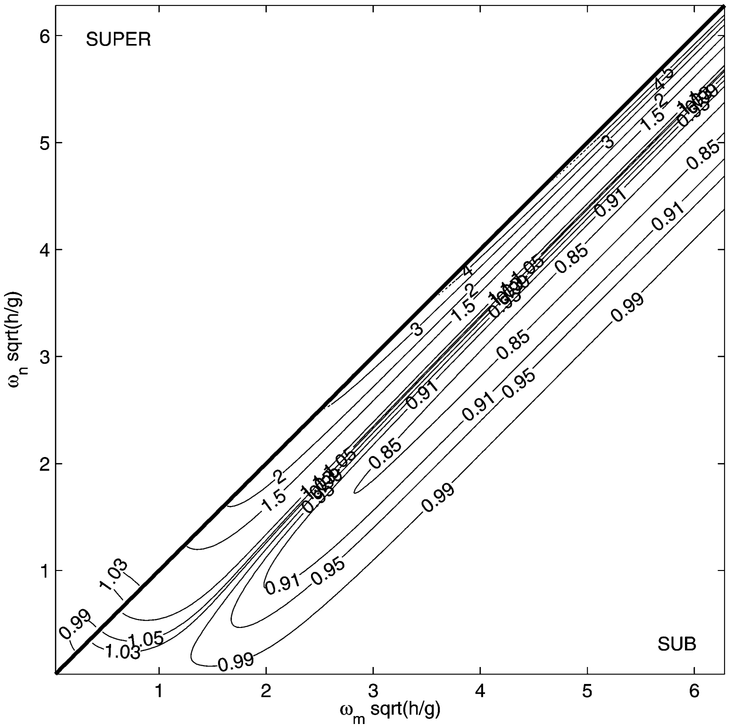

Fig. 3. Second-order bichromatic transfer functions for evolution equations invoking the resonance assumption. The values are normalised with the exact transfer function.

for large forcing frequencies. Hence the transfer is dominated by the first term in $\widetilde{W}_{s,p-s}$ which does not involve the H operator. The sub-harmonic transfer is under-predicted in a region parallel to the diagonal and over-predicted along the diagonal. Lines being parallel to the diagonal represent constant receiving frequencies. Parallel lines close to and below the diagonal represent long waves forced sub-harmonically by waves having close frequencies.

5. Speeding up the calculations using FFT

The computational effort of a direct evaluation of the right-hand side of (53) is $\mathrm{O}(M^2N^2)$. For a large number of frequencies (corresponding to a long time series) or a large number of y wave modes, this makes the model infeasible to apply. This problem has traditionally limited the use of evolution equations of the above type.

For the one-dimensional Boussinesq evolution equations of Madsen and Sorensen [7], Bredmose et al. [14] showed that the nonlinear terms can be calculated using Fast Fourier Transforms at a computational effort of $\mathrm{O}(N\log N)$. This method of speeding up the calculation of a convolution sum has been used extensively within spectral methods for partial differential equations, see e.g. Canuto, Hussaini, Quarteroni and Zang [30]. In the field of evolution equations, Dalrymple et al. [25] used this technique to calculate a term corresponding to the second term on the right-hand side of (44). This term is associated with the non-uniformity of depth in the lateral direction. However, for treatment of the nonlinear terms within spatial evolution equations for wave propagation, this speed-up technique appears to be new. Unfortunately, this method of speeding up the calculations cannot be applied directly to the new 'exact' models. We detail this later in this section. First, however, we describe the method of the numerical speed-up for the 'resonant' models.

Consider the very first term in the nonlinear sums of (53)

$$\mathrm{term}_1 = \mathrm{i}\varepsilon \sum_{s=p-N}^{N} \sum_{t=\max\{l-M,-M\}}^{\min\{l+M,M\}} \left\{ \bar{k}^x_{s,t} \frac{g}{2\omega_s\omega_{p-s}} \bar{\mathbf{k}}_{s,t}\cdot\bar{\mathbf{k}}_{p-s,l-t} a_{s,t} a_{p-s,l-t} \times \mathrm{e}^{-\mathrm{i}\int(\bar{k}^x_{s,t}+\bar{k}^x_{p-s,l-t}-\bar{k}^x_{p,l})\,\mathrm{d}x} \right\}. \tag{68}$$

For simplicity we evaluate the dot product of the two wave number vectors, and consider only the first term arising. The other term can be treated similarly as the first—as is also the case for all the other terms in the convolution sums. We write the new term as

$$\mathrm{term}_{11} = \mathrm{i}\varepsilon \frac{g}{2} \mathrm{e}^{\mathrm{i}\int \bar{k}^x_{p,l}\,\mathrm{d}x} \sum_{s=p-N}^{N} \sum_{t=\max\{l-M,-M\}}^{\min\{l+M,M\}} \left\{ \frac{(\bar{k}^x_{s,t})^2}{\omega_s} a_{s,t}\, \mathrm{e}^{-\mathrm{i}\int \bar{k}^x_{s,t}\,\mathrm{d}x} \right\} \left\{ \frac{\bar{k}^x_{p-s,l-t}}{\omega_{p-s}} a_{p-s,l-t}\, \mathrm{e}^{-\mathrm{i}\int \bar{k}^x_{p-s,l-t}\,\mathrm{d}x} \right\}. \tag{69}$$

Inspired by this expression, we define

$$s_1 = \sum_{p=-N}^{N} \sum_{l=-M}^{M} \left\{ \frac{(\bar{k}^x_{p,l})^2}{\omega_p} a_{p,l}\, \mathrm{e}^{-\mathrm{i}\int \bar{k}^x_{p,l}\,\mathrm{d}x} \right\} \mathrm{e}^{\mathrm{i}p\omega t}\, \mathrm{e}^{-\mathrm{i}k^y_l y}, \tag{70}$$

$$s_2 = \sum_{p=-N}^{N} \sum_{l=-M}^{M} \left\{ \frac{\bar{k}^x_{p,l}}{\omega_p} a_{p,l}\, \mathrm{e}^{-\mathrm{i}\int \bar{k}^x_{p,l}\,\mathrm{d}x} \right\} \mathrm{e}^{\mathrm{i}p\omega t}\, \mathrm{e}^{-\mathrm{i}k^y_l y}. \tag{71}$$

which are functions of t and y. Further, we define the Fourier amplitudes of their product as

$$s_1 s_2 \equiv \sum_{p=-2N}^{2N} \sum_{l=-2M}^{2M} [\widehat{s_1 s_2}]_{p,l}\, \mathrm{e}^{\mathrm{i}p\omega t}\, \mathrm{e}^{\mathrm{i}k^y_l y}. \tag{72}$$

The convolution theorem then states that the double summation in (69) is equal to $[\widehat{s_1 s_2}]_{p,l}$, and we thus have

$$\mathrm{term}_{11} = \mathrm{i}\varepsilon \frac{g}{2} [\widehat{s_1 s_2}]_{p,l}\, \mathrm{e}^{\mathrm{i}\int \bar{k}^x_{p,l}\,\mathrm{d}x}. \tag{73}$$

This is the key point of the speed-up technique. Given the values of $a_{p,l}$ for $1 \leqslant p \leqslant N$ and $-M \leqslant l \leqslant M$, and the associated wave numbers and angular frequencies, s_1 and s_2 can be calculated by an inverse Fourier transformation in the y-direction followed by an inverse Fourier transformation in time. This gives the values of s_1 and s_2 on a grid in the (y,t) plane, and the product $s_1 s_2$ can be calculated for each (y,t). Applying two forward Fourier transformations, one in time and one in the y-direction then gives the values of $[\widehat{s_1 s_2}]_{p,l}$ needed. If all Fourier transformations are carried out using FFTs, term_{11} can thus be calculated with a computational effort of $\mathrm{O}((M \log M)(N \log N))$. The same procedure can be applied to all the other terms in the 'resonant' versions of the models (53) and (44). The second term on the right-hand sides of these models can be treated similarly, although less complicated, since it only involves a single convolution.

As can be seen in (72), the quadratic terms contain Fourier components with frequencies up to double as large as those described in the spectrum resolved. As these higher frequencies do not belong to the spectrum resolved, care must be taken to avoid any aliasing from these frequencies onto the frequency range modelled. Aliasing among the frequencies $1,\dots,N$ in time and $-M,\dots,M$ in the y-direction is avoided if more than 3N points are used for describing the time variation of $s_1 s_2$ and more than 3M points are used to describe the y-variation. Practically, as the FFT algorithm is most efficient for signal lengths being a product of small prime factors, the number of points in (time,y-direction) should be chosen as the smallest products of this type, exceeding $(3N, 3M)$. More details on aliasing can be found in e.g. Canuto et al. [30].

While the above speed-up technique is easily applied to the 'resonant' models, it cannot be applied to the 'exact' models. The reason is that $\widetilde{\mathrm{H}}(h\boldsymbol{\nabla}, \bar{\mathbf{k}}_{p,l}h)$ with $\boldsymbol{\nabla} = -\mathrm{i}(\bar{\mathbf{k}}_{s,t} + \bar{\mathbf{k}}_{p-s,l-t})$ cannot be written as a product of independent factors, each depending solely on one of the index pairs (p,l), (s,t) and $(p-s, l-t)$ as in (69). It is therefore not possible to define series like s_1 and s_2 for an evaluation of the nonlinear terms in the time domain.

Hence, the 'resonant' models are more feasible for practical use. We have already found that the second-order transfer for these models is generally close to that of the 'exact' models for unidirectional wave propagation. We now validate and compare the models for two test examples.

6. Application to wave propagation over a submerged bar

We validate the models by applying them to an example of weakly nonlinear, unidirectional wave propagation over a submerged bar. We base the test on the experiments of Beji and Battjes [15]. Irregular waves of different significant wave height, peak frequency and spectral shape were propagated over a submerged bar. The depth of the wave flume was 0.4 m, while on the bar top the depth was 0.1 m. The upward slope of the bar was 1/20, while the downward slope was 1/10. The surface elevation was sampled at 10 Hz in eight stations along the flume. The bathymetry is sketched in Fig. 4 where the stations for the measurements are also marked. We here pick two tests of non-breaking waves.

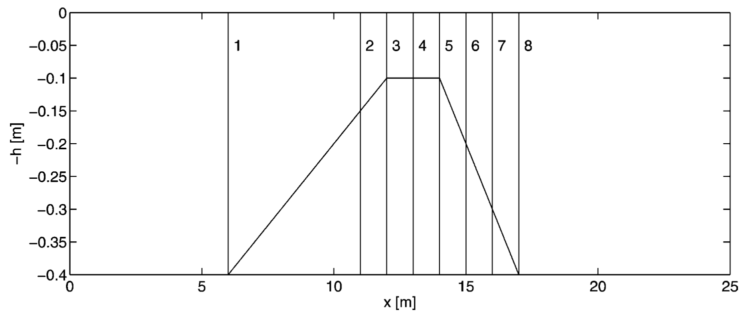

Fig. 4. Bathymetry and stations for the experiments of Beji and Battjes [15].

6.1. A test on long waves

For the first test, the incident waves are described by a JONSWAP spectrum with a peak frequency of 0.4 Hz and a significant wave height of $H_s = 2.9$ cm. A JONSWAP spectrum (JOint North Sea Wave Project) is a modification of the Pierson–Moscowitz spectrum, see e.g. Sumer and Fredsøe [31]. The time series has a length of $T_{\mathrm{dur}} = 899.68$ s, corresponding to a frequency resolution of $f_1 = 1/T_{\mathrm{dur}} = 1.11 \times 10^{-3}$ Hz. The wave model (53) in its unidirectional form was run with 1800 frequencies corresponding to a maximum frequency of 2 Hz. The Fourier amplitudes of the experimental time series in station 1 was used as initial condition, and the evolution equations were integrated with a constant spatial step length of 0.1 m. Reducing the step length to 0.05 m had no significant impact on the results. Note that when solving evolution equations, the choice of step length is not governed by a Courant number criterion as for time domain models. If the present test was to be modelled using a time domain model, resolving the shortest wave by two points per wave period would give a time step of 0.25 s. With the current choice of spatial step length of 0.1 m, this would correspond to a Courant number of nearly 5 (!) in the deep part of the domain. This avoidance of the Courant number criterion is one of the reasons for the computational efficiency of evolution equations.

Results from the ‘exact’ model are shown together with experimental time series for stations 3,5 and 8 in Fig. 5. These stations correspond to the two upper corners of the bar and the lower corner after the bar. The time interval depicted represents a typical part of the time series.

The record from station 3 consists of two wave groups with a single isolated wave in between. The high waves have an asymmetric shape, corresponding to a forward leaning of their spatial profiles, resulting from the shoaling process on the bar front. The model results match the data well, except for a few spurious oscillations following the tallest wave crests.

When the waves reach the flat bottom at the bar top, the forward leaning wave shape is no longer stable. The waves change their shape through nonlinear interactions which from a spectral point of view happens through energy exchange between the different frequency components. At the bar top the water is fairly shallow, ($kh = 0.32$ for the peak frequency) and the quadratic interactions therefore approach near-resonance, (see e.g. Phillips [3]). As a result the shape of the waves changes rather dramatically over the bar top. In station 5, the recorded waves are thus seen to be more spiky when compared to station 3 and do not show much asymmetry. The numerical results reproduce the data well, although for the highest waves the crests are seen to be followed by a spurious trough. The highest waves also exhibit small phase errors, the numerical waves arriving slightly too early.

On the down-hill side of the bar, the waves are subject to de-shoaling. In this process some of the high-frequency content of the waves is released as free harmonics, thus resulting in a higher content of high-frequency wave energy behind the bar than in front of the bar. This is clearly seen in the time series of station 8, were the typical wave period is apparently half the period of the waves seen in station 3. The numerical model results exhibit this behaviour as well. Some of the waves are reproduced with reasonable accuracy, while for other waves, phase errors and amplitude errors are seen. In general, the wave model gives a fair reproduction of the overall wave pattern.

Starting from linear theory, a second-order model like the one used here, is the first step towards a fully nonlinear calculation of the wave evolution. It is therefore interesting to compare the performance of the present wave model to results of linear wave theory. Thus in Fig. 6, numerical results from a linear run of (53) is shown together with the experimental data. When comparing to the second-order results in Fig. 5, it is evident that the linear waves show a lack of asymmetry in station 3, while in station 5, the wave profiles are too broad, have too deep troughs and too small crest heights. These observations are clear indications of a too low content of higher harmonics. Consequently at the down-hill side of the bar, station 8, no reduction of the apparent wave period is obtained and the linearly predicted wave field shows little resemblance with the experimental data. For this test, the second-order terms thus provide a clear improvement from linear theory.

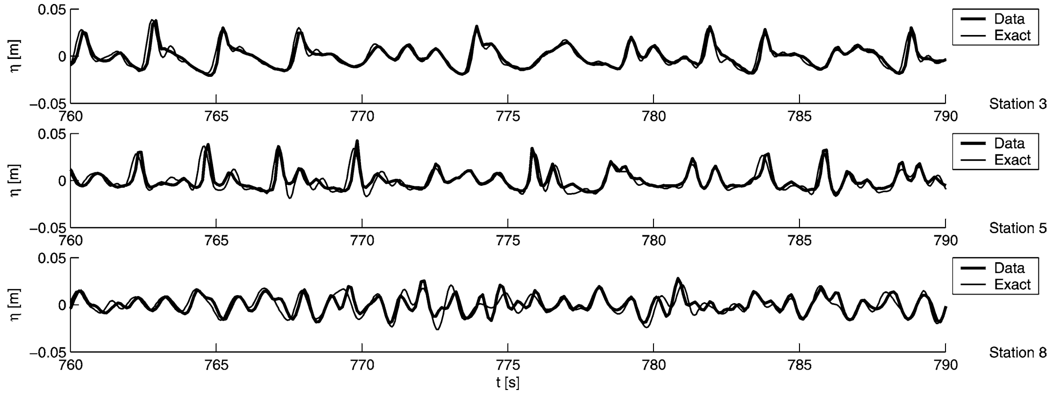

Fig. 5. Time series in three stations for the long wave test of Beji and Battjes [15]. Experimental data and results of 'exact' model.

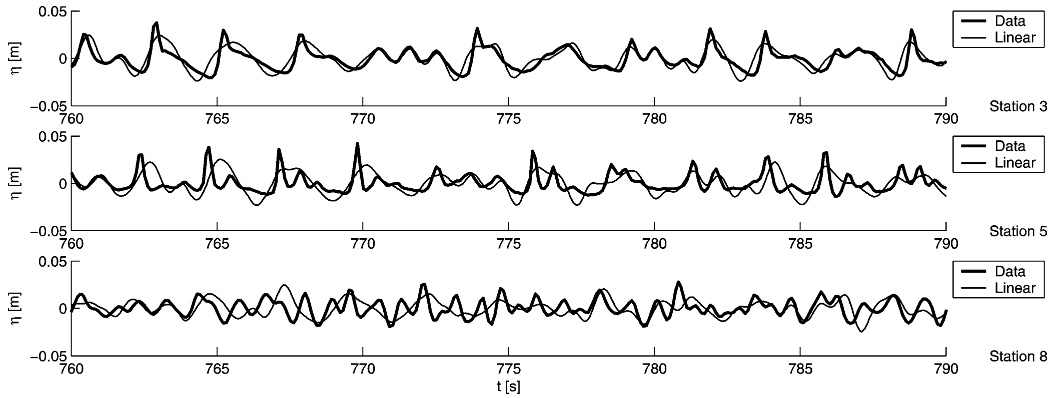

Fig. 6. Time series in three stations for the long wave test of Beji and Battjes [15]. Experimental data and results of linearised model.

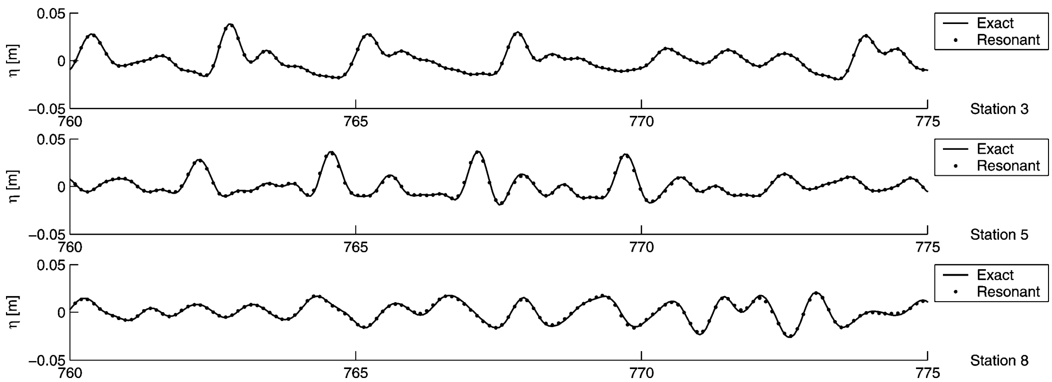

Fig. 7. Time series in three stations for the long wave test of Beji and Battjes [15]. Comparison between 'exact' and 'resonant' model.

Results of the 'exact' and 'resonant' models are compared in Fig. 7. Only the first half of the time interval of Figs. 5 and 6 is shown, since the last half interval shows an even smaller deviation. We see that the deviation between the model results is hardly discernible. Thus compared to the deviation between the model results and experimental data, the difference between the 'exact' and 'resonant' model is insignificant.

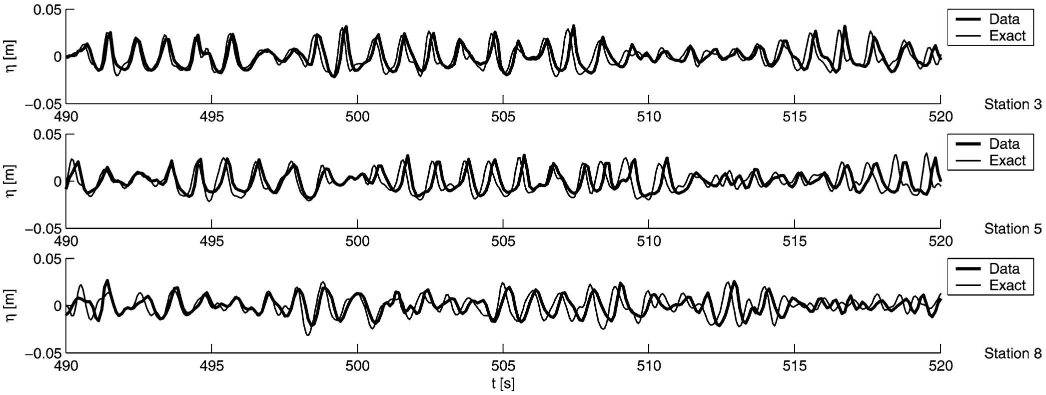

Fig. 8. Time series in three stations for the short wave test of Beji and Battjes [15]. Experimental data and results of 'exact' model.

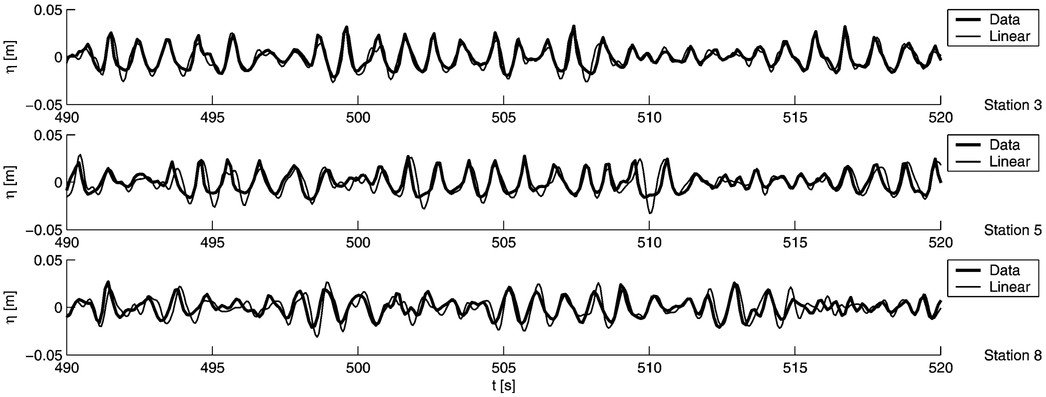

Fig. 9. Time series in three stations for the short wave test of Beji and Battjes [15]. Experimental data and results of linearised model.

6.2. Shorter waves

For the second test chosen, the incoming wave spectrum is a JONSWAP spectrum with a peak frequency of 1 Hz and a significant wave height of 4.1 cm. The duration of the time series is $T_{\mathrm{dur}} = 899.68$ s and the evolution equations were solved with 2700 frequencies, corresponding to a maximum frequency of 3 Hz.

First we examine the results for the time interval $t = [490; 520]$ s. Results of the 'exact' model are compared to experimental data in Fig. 8, while results of a linear model run are compared to data in Fig. 9. In general, both models are able to capture the individual waves. However, the waves calculated with the nonlinear evolution equations show a forward phase shift when compared to the data. This phase shift is not present for the linear results and is thus a consequence of nonlinearity. In station 5, the results of the linear model in general exhibit too deep wave troughs. This behaviour is not seen for the results of the nonlinear evolution equations, although for this station the phase shift has increased due to accumulative effects. For station 8, both models reproduce the overall variation of the wave field, although phase errors and spurious high-frequency oscillations are present in the results.

We now focus on the results for a single tall wave group, covering the time interval $t = [325; 340]$ s. Numerical results of the nonlinear evolution equations are compared to the measured time series in Fig. 10, while linear results and data are compared in Fig. 11. For station 3, the asymmetry and spikiness of the measured waves indicate the presence of second harmonic energy in the wave spectrum. The nonlinear evolution equations capture the appearance of the second harmonics and thus reproduce the shape of the waves with a good improvement from linear theory. The same holds for the results of station 5. For these stations phase errors are evident for both models, the linear model results exhibiting a backward phase shift and the nonlinear model exhibiting a forward phase shift in time. This shows that there is a nonlinear contribution to the phase speed in the data, and that the nonlinear model overestimates this contribution. For station 8, these phase shifts accumulate for both models and thus make a judgement of the reproduction of wave shape difficult.

Results of the 'exact' and the 'resonant' model are compared in Fig. 12. We see that for the smaller waves the deviations are insignificant, while for the larger waves, some differences in wave shape occur. For these large waves, however, the deviation to

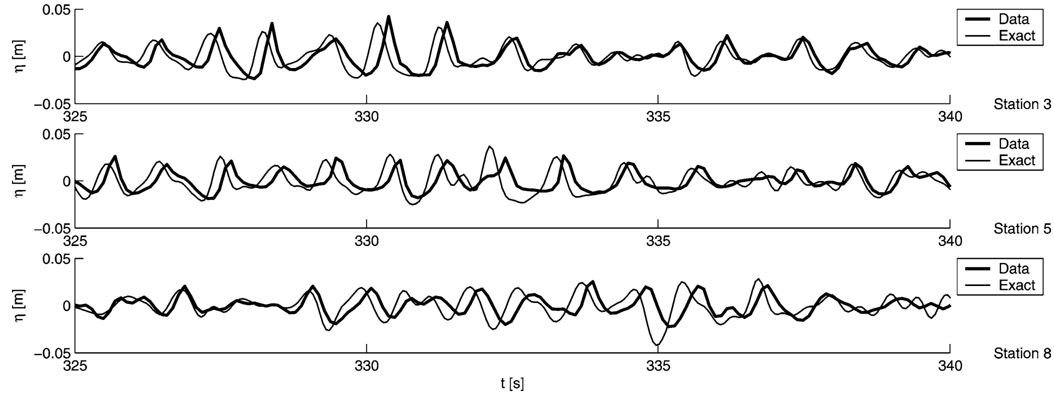

Fig. 10. Time series in three stations for the short wave test of Beji and Battjes [15]. Experimental data and results of 'exact' model.

p

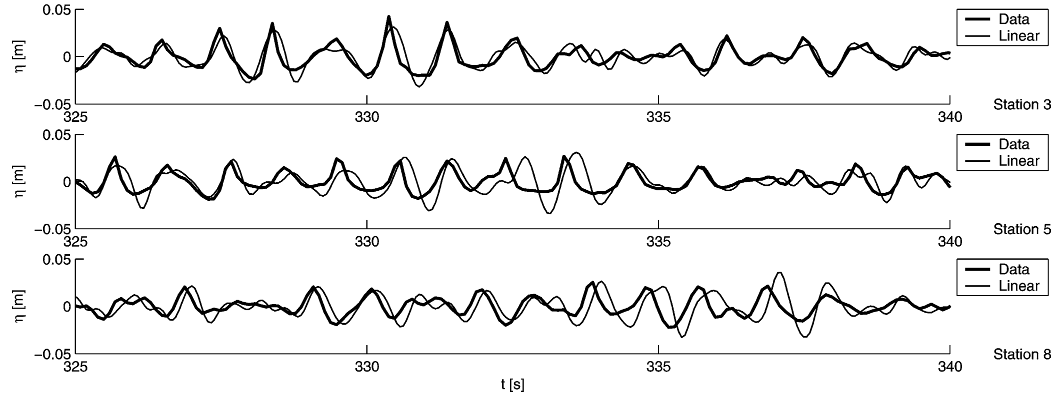

Fig. 11. Time series in three stations for the short wave test of Beji and Battjes [15]. Experimental data and results of linearised model.

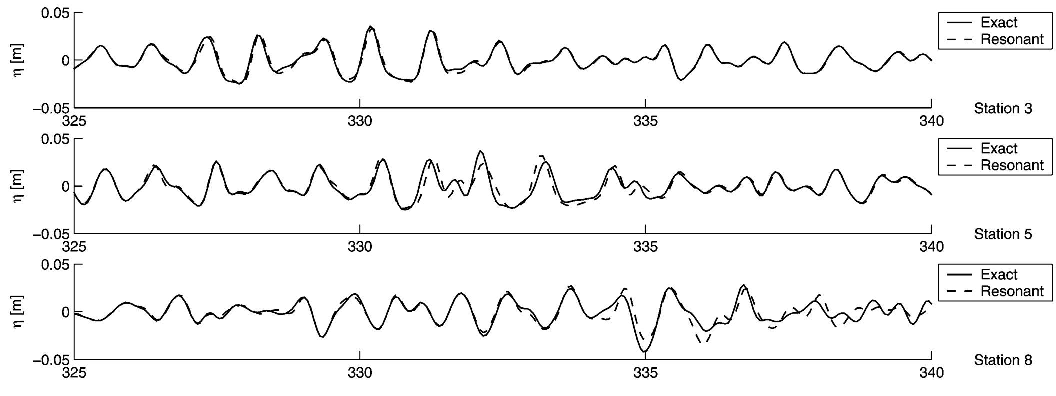

Fig. 12. Time series in three stations for the short wave test of Beji and Battjes [15]. Results of 'exact' model and 'resonant' model.

the measured data is relatively large. From a modelling point of view, the results of the two models can therefore be considered of equal quality for this test case.

Although the above tests show that the second-order terms make an improvement over linear theory with respect to wave shape, the results of the second test gives evidence that the amplitude dispersion is over-predicted in the model. This leads to undesirable accumulative phase errors. Motivated by these observations, we thus investigate the amplitude dispersion within the models in the following section.

7. Third-order transfer and embedded amplitude dispersion

The above results suggest that the amplitude dispersion in the models formulated in η is over-predicted. Kaihatu [20] investigated the nonlinear contribution to the phase speed in the 'resonant' model formulated in ϕ by calculating fully nonlinear regular wave solutions. For small waves it was found that the nonlinear phase speed exceeds the phase speed of Stokes third-order waves (presumably with a zero Eulerian mean current below wave trough level) for $kh \lesssim 1.5$, where k is the linear wave number. For larger values of kh, the nonlinear phase speed was found to be smaller than for Stokes waves. For shallow water waves, comparisons with stream function theory confirmed the over-prediction of the phase speed in shallow water, although the transition from over-prediction to under-prediction of the phase speed occurred at a much smaller wave number, $kh \approx 0.3$.

It is desirable to investigate the amplitude dispersion of the model formulated in η as well. We choose to use a third-order Stokes-type analysis for this, which additionally to results for the amplitude dispersion and third-order transfer of the model yields insight into the process that creates the nonlinear contribution to the phase speed. We restrict the analysis to unidirectional wave propagation and follow the approach of Bredmose et al. [14]. We look for a solution of the form

$$\eta(x,t) = \frac{\varepsilon}{k_1}\cos\theta + \frac{\varepsilon^2}{k_1}\tilde{A}_2\cos 2\theta + \frac{\varepsilon^3}{k_1}\tilde{A}_3\cos 3\theta \tag{74}$$

with

$$\theta = \omega t - k_1 x, \quad \omega = \omega_1(1+\varepsilon^2\omega_{13}) \tag{75}$$

and where $\varepsilon = k_1 A_1$ is assumed small. The coefficients $(\tilde{A}_2, \tilde{A}_3, \omega_{13})$ are dimensionless functions of kh, being of order $O(1)$ in the ε-hierarchy. As reference solution, we use Stokes third-order waves with a zero net mass flux ($c_s = 0$), corresponding to unidirectional wave propagation towards a beach. This solution is given in Fenton [32] and reads in our notation

$$\tilde{A}_3 = 3\frac{1+3S+3S^2+2S^3}{8(1-S)^3}, \tag{76}$$

$$\omega_{13} = \frac{2+7S^2}{4(1-S)^2} - \frac{1}{2}\frac{1}{\kappa\tanh\kappa} \tag{77}$$

with $\kappa = kh$ and $S = \operatorname{sech} 2\kappa$. Omission of the last term in ω_{13} leads to the solution corresponding to a zero Eulerian mean velocity below wave trough level ($c_E = 0$). The ratio of these two solutions for ω_{13} can be as large as 2.5, and it is therefore important to specify which reference solution is used. We note that $\tilde{A}_3$ is independent of the mass flux.

In evolution equations, ω_p are fixed numbers and are therefore not allowed to be modified by nonlinear effects as in (75). The nonlinear modification of the wave speed therefore enters through a change of the effective wave number, and we thus search for a solution of the form (74) but with

$$\theta = \omega_1 t - kx, \quad k = k_1(1-\varepsilon^2 k_{13}). \tag{78}$$

Matching the solution ansatz (74) with the expansion (18) gives

$$a_1 = \frac{1}{2}\frac{\varepsilon}{k_1}\,\mathrm{e}^{-\mathrm{i}(k-k_1)x}, \quad a_2 = \frac{1}{2}\frac{\varepsilon^2}{k_1}\tilde{A}_2\,\mathrm{e}^{-\mathrm{i}(2k-k_2)x}, \quad a_3 = \frac{1}{2}\frac{\varepsilon^3}{k_1}\tilde{A}_3\,\mathrm{e}^{-\mathrm{i}(3k-k_3)x}. \tag{79}$$

For constant depth and unidirectional wave propagation, the evolution equations (53) take the form

$$a_{p,x} = \mathrm{i}\sum_{s=p-N}^{N} \mathrm{W}_{s,p-s} a_s a_{p-s}\,\mathrm{e}^{-\mathrm{i}(k_s+k_{p-s}-k_p)x} \tag{80}$$

where, again, we have adopted the two-index notation for the kernel function $\widetilde{\mathrm{W}}$. In the presence of only three harmonics, (80) form the system

$$a_{1,x} = 2\mathrm{i}\mathrm{W}_{2,-1} a_2 a_{-1}\,\mathrm{e}^{-\mathrm{i}(k_2-2k_1)x}, \tag{81}$$

$$a_{2,x} = \mathrm{i}\mathrm{W}_{1,1} a_1^2\,\mathrm{e}^{-\mathrm{i}(2k_1-k_2)x}, \tag{82}$$

$$a_{3,x} = 2\mathrm{i}\mathrm{W}_{2,1} a_1 a_2\,\mathrm{e}^{-\mathrm{i}(k_1+k_2-k_3)x}, \tag{83}$$

and insertion of (79) now gives a hierarchy of equations in ε. The $(\varepsilon^0, \varepsilon^1)$-equations are identically satisfied, while at $O(\varepsilon^2)$, (82) yields the solution for $\tilde{A}_2$. At $O(\varepsilon^3)$, (81) gives the solution for k_{13}, while (83) gives the solution for $\tilde{A}_3$. The solutions are

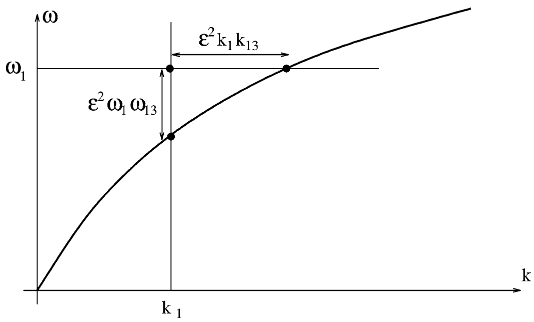

Fig. 13. A nonlinear wave and the two linear waves having same wave number and same frequency, respectively.

$$\tilde{A}_2 = \frac{W_{1,1}}{2k_1(k_2 - 2k_1)}, \tag{84}$$

$$\tilde{A}_3 = \frac{W_{2,1}W_{1,1}}{2k_1^2(k_2 - 2k_1)(k_3 - 3k_1)}, \tag{85}$$

$$k_{13} = \frac{W_{2,-1}W_{1,1}}{2k_1^3(k_2 - 2k_1)} \tag{86}$$

where the result for $\tilde{A}_2$ is consistent with the bichromatic transfer function (67) derived in Section 4.

To relate k_{13} to ω_{13}, we consider the sketch in Fig. 13. Here a curve representing the linear dispersion relation for water waves is drawn, and a nonlinear wave is represented by a point positioned above this curve. If this nonlinear wave is described through a change of ω, the nonlinear wave originates from the linear wave having the same wave number (k_1), and the vertical distance between this wave and the nonlinear wave is $\varepsilon^2\omega_1\omega_{13}$. Similarly, if the nonlinear wave is described through a change of the wave number, it originates from the linear wave having the same angular frequency (ω_1) and the horizontal distance between this wave and the nonlinear wave is $\varepsilon^2 k_1 k_{13}$. We can relate k_{13} to ω_{13} by considering the triangle defined by these two linear waves and the nonlinear wave. As the slope of the dispersion curve is $\frac{\partial\omega}{\partial k}$ we have $\varepsilon^2\omega_1\omega_{13} = \varepsilon^2 k_1 k_{13}\frac{\partial\omega}{\partial k}$, and thereby

$$\omega_{13} = \frac{c_g}{c_{\mathrm{lin}}} k_{13}. \tag{87}$$

Note that since the deviation between the wave numbers and angular frequencies for the linear and nonlinear waves are of order $\mathrm{O}(\varepsilon^2)$, c_g, the group velocity, and c_{lin}, the linear phase speed, can be evaluated in any of the three points as desired.

7.1. Analysis of model in ϕ

As (44) and (53) are only consistent to second order, their third-order properties are not identical. Hence we need to analyse (44) separately. In its unidirectional form, we write (44) as

$$b_{p,x} = -\sum_{s=p-N}^{N} \mathrm{U}_{s,p-s} b_s b_{p-s}\, \mathrm{e}^{-\mathrm{i}(k_s + k_{p-s} - k_p)x} \tag{88}$$

where $\mathrm{U}_{s,p-s} \equiv \mathrm{H}(h\nabla, k_p h)\mathrm{F}^{(2)}_{s,p-s}$. We insert the solution ansatz

$$b_1 = \frac{1}{2}\frac{\mathrm{i}g}{\omega_1}\frac{\varepsilon}{k_1}\,\mathrm{e}^{-\mathrm{i}(k-k_1)x}, \quad b_2 = \frac{1}{2}\frac{\mathrm{i}g}{\omega_1}\widetilde{\Phi}_2\frac{\varepsilon^2}{k_1}\,\mathrm{e}^{-\mathrm{i}(2k-k_2)x}, \quad b_3 = \frac{1}{2}\frac{\mathrm{i}g}{\omega_1}\widetilde{\Phi}_3\frac{\varepsilon^3}{k_1}\,\mathrm{e}^{-\mathrm{i}(3k-k_3)x} \tag{89}$$

where $\widetilde{\Phi}_2$ and $\widetilde{\Phi}_3$ are dimensionless functions of kh and where again $k = k_1(1 - \varepsilon^2 k_{13})$. Insertion into (88) leads to

$$\widetilde{\Phi}_2 = -\frac{g}{\omega_1}\frac{\mathrm{U}_{1,1}}{2k_1(k_2 - 2k_1)}, \tag{90}$$

$$\widetilde{\Phi}_3 = \left(\frac{g}{\omega_1}\right)^2 \frac{\mathrm{U}_{1,1}\mathrm{U}_{2,1}}{2k_1^2(k_2 - 2k_1)(k_3 - 3k_1)}, \tag{91}$$

$$k_{13} = -\left(\frac{g}{\omega_1}\right)^2 \frac{\mathrm{U}_{1,1}\mathrm{U}_{2,-1}}{2k_1^3(k_2 - 2k_1)}, \tag{92}$$

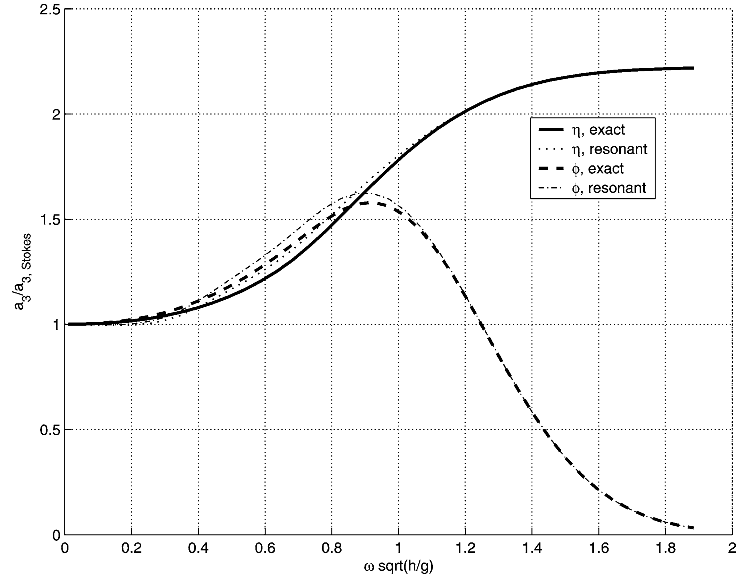

Fig. 14. $\tilde{A}_3$ for fully dispersive evolution equations, normalised by $\tilde{A}_3$ for Stokes waves. Results for the resonance assumption are shown as well.

which have a clear similarity with (84)–(86). We now calculate the free surface elevation amplitudes corresponding to (89) using the second-order transformation (48). The quadratic terms in this transformation can easily be expressed in terms of potential amplitudes by using the linear part of the transformation. Hereby a transformation expressing $\hat{\eta}_p$ in terms of only potential amplitudes is obtained. Using this transformation we get

$$\hat{\eta}_1 = \frac{1}{2}\frac{\varepsilon}{k_1}\,\mathrm{e}^{-\mathrm{i}kx} + \mathrm{O}(\varepsilon^3), \tag{93}$$

$$\hat{\eta}_2 = -\frac{1}{2}\left(\frac{g}{\omega_1}\frac{\mathrm{U}_{1,1}}{k_1(k_2-2k_1)} + \frac{\omega_1}{gk_1}\mathrm{T}^{(2)}_{1,1}\right)\frac{\varepsilon^2}{k_1}\,\mathrm{e}^{-2\mathrm{i}kx}, \tag{94}$$

$$\hat{\eta}_3 = \frac{1}{2}\left(\frac{3}{2}\left(\frac{g}{\omega_1}\right)^2\frac{\mathrm{U}_{1,1}\mathrm{U}_{2,1}}{k_1^2(k_2-2k_1)(k_3-3k_1)} + 3\frac{\mathrm{U}_{1,1}\mathrm{T}^{(2)}_{2,1}}{k_1^2(k_2-2k_1)}\right)\frac{\varepsilon^3}{k_1}\,\mathrm{e}^{-3\mathrm{i}kx} \tag{95}$$

where the results for $(\hat{\eta}_1, \hat{\eta}_2)$ are consistent with the results of the analysis of the model formulated in η (53), while the result for $\hat{\eta}_3$ is not. The first term in the above result for $\hat{\eta}_3$ results from the linear transformation of $\hat{\phi}_3$, while the second term is produced by the quadratic part of the transformation (48).

7.2. *Results of analysis*

We can now compare the third-order transfer and embedded amplitude dispersion of the evolution equations to the reference solution of Stokes third-order theory. In Fig. 14 the third-order transfer function $\tilde{A}_3$ of the evolution equations formulated in the amplitudes of the free surface elevation as well as the evolution equations formulated in the amplitudes of the still water velocity potential is plotted. All curves are normalised with the reference solution of Stokes third-order wave theory. The transfer is seen to be over-predicted for the model in η. In shallow water, the model agrees with Stokes wave theory, but in deep water, the transfer function converges towards a value of around 2.2 times that of Stokes waves. For the model in ϕ, the transfer is first over-predicted in shallow and intermediate water and then under-predicted decaying to zero in deep water. The largest over-prediction is 58% and occurs for $\omega\sqrt{h/g} = 0.92$, while the transition to the region of under-prediction occurs in $\omega\sqrt{h/g} = 1.25$. The influence of the resonance approximation is illustrated as well and is seen to be small. This is explained by the expression for $\tilde{A}_3$ which consists of a product of two super-harmonic interaction coefficients $\widetilde{\mathrm{W}}_{1,1}$ and $\widetilde{\mathrm{W}}_{2,1}$. For super-harmonic interactions, the resonance approximation does not imply significant changes to the transfer function, as can be seen in Fig. 3.

To analyse the embedded amplitude dispersion, we compare ω_{13} of the evolution equations to ω_{13} for Stokes third-order waves on a zero net mass flux in Fig. 15. The plot shows that the evolution equations over-predict the amplitude dispersion

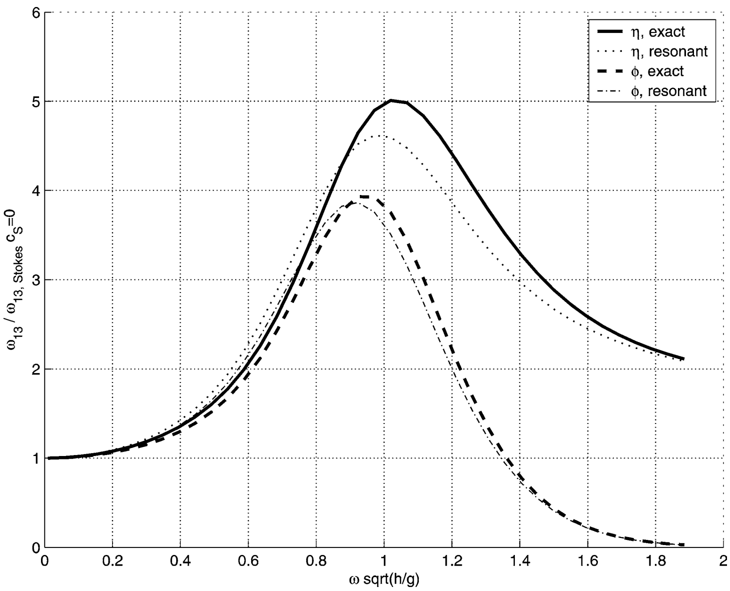

Fig. 15. ω_{13} for fully dispersive evolution equations, normalised by ω_{13} for Stokes waves with $c_S = 0$. Results for the resonance assumption are shown as well.

severely. The equations formulated in η over-predict the amplitude dispersion by a factor of 5 for $\omega\sqrt{h/g} = 1.03$. Towards deep water, the amplitude dispersion decays, but still in $\omega\sqrt{h/g} = 2\pi$ (not shown in the figure) corresponding to $kh = 39.5$, ω_{13} is more than 1.5 times as large as for Stokes waves. For the short wave calculation of Section 6.2, $\omega(h/g)^{1/2}$ varies between 1.27 and 0.63 for the peak frequency, and the third-order analysis therefore explains the over-prediction of amplitude dispersion observed.

For the evolution equations in ϕ, the analysis shows a similar over-prediction in shallow and intermediate water, while for deeper water the amplitude dispersion decays towards zero. The largest over-prediction occurs for $\omega\sqrt{h/g} = 0.95$, where ω_{13} is nearly four times as large as for Stokes waves. The transition between over-prediction and under-prediction occurs for $\omega\sqrt{h/g} = 1.36$. The effect of the resonance approximation is small, and most pronounced for the model in η. The decay of ω_{13} in deep water for the model in ϕ can be explained by the decay of $\widetilde{F}^{(2)}_{s,p-s}$ for super-harmonic forcing by large frequencies. Thus for deep water, the interaction coefficient for super-harmonic interaction vanishes, making ω_{13} decay, see (86).

As already noted, the use of a reference solution for a zero net mass flux ($c_S = 0$) gives a larger over-prediction of the amplitude dispersion than if the reference solution for a zero mean Eulerian velocity below wave trough level is used ($c_E = 0$). The effect is illustrated in Fig. 16, where ω_{13} for the 'exact' model in η is plotted, normalised with either of the two reference solutions. The two reference solutions can differ by up to a factor of 2.5, as can be seen in the plot. For both reference solutions, however, the amplitude dispersion is over-predicted by the model formulated in η. For the 'resonant' model formulated in ϕ (not included in the figure), the transition from over-prediction to under-prediction of the amplitude dispersion for $c_E = 0$ occurs at $\omega\sqrt{h/g} = 1.16$ corresponding to $kh = 1.49$. This agrees very well with the findings of Kaihatu [20].

Given that the evolution equations derived are correct to second order, it may seem surprising that the third-order properties analysed deviate significantly from the reference solution. However, as the derivation of the models has only been carried out with second-order accuracy, the third-order properties of the models are rather arbitrary.

Together with the simulations of Section 6 the above findings show that fully dispersive evolution equations may be less successfully applied to wave fields where third-order properties are important or at least to wave fields having a large spectral content in the frequency range of strongly over-predicted amplitude dispersion. While a general over-prediction of the third-order transfer may be tolerable, the over-prediction of amplitude dispersion leads to undesirable accumulative phase errors. An extension to third order would cure these problems, but seems infeasible if the numerical efficiency is to be retained. However, an approximate correction term may possibly cure the problems of amplitude dispersion, thus rendering a model still consistent to second order and with improved, although not exact, third-order properties. Such a modification is subject to current investigations.

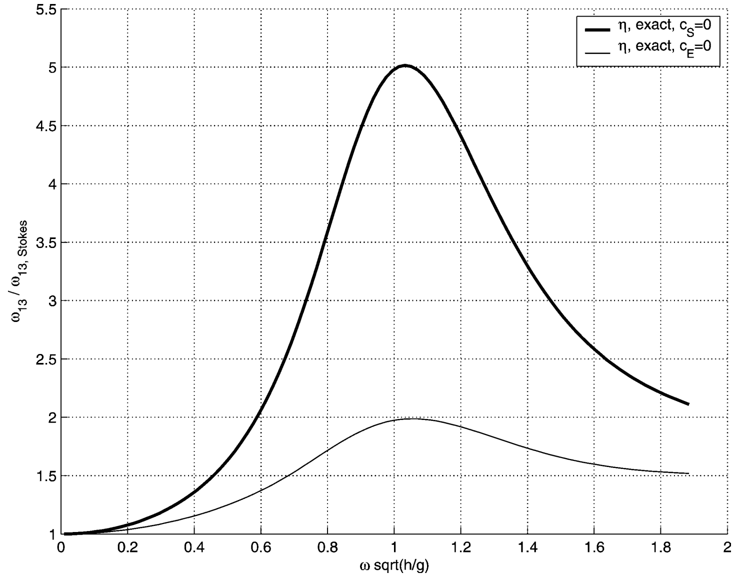

Fig. 16. ω_{13} for the 'exact' version of the evolution equations (53). The two curves are obtained by normalising with ω_{13} for third-order Stokes waves with a zero net mass flux ($c_S = 0$) and a zero Eulerian mean flux velocity below wave trough level ($c_E = 0$), respectively.

8. Summary and discussion

A new derivation of second-order fully dispersive evolution equations with no assumptions on the vertical structure of the velocity field has been presented. The equations are valid for weakly nonlinear wave propagation at angles up to $\pm 90°$ from the main direction of propagation with a weak deviation from straight and parallel bottom contours. The models are formulated in the complex Fourier amplitudes of the still water potential or the complex Fourier amplitudes of the free surface elevation and have, as a novelty, exact second-order bichromatic transfer functions. By utilising the 'resonance assumption', the models of Agnon et al. [10], Kaihatu and Kirby [11] and Eldeberky and Madsen [12] are recovered.

The second-order bichromatic transfer functions of the models have been derived using a perturbation analysis. For the 'exact' models the transfer functions are identical to the reference solution of Sharma and Dean [13]. For unidirectional wave propagation the bichromatic transfer of the 'resonant' models is generally close to the exact transfer function, especially for super-harmonics.

The numerical efficiency related to the solution of the 'resonant' models can be improved by using Fast Fourier Transforms to evaluate the nonlinear terms. This leads to a tremendous reduction in the computational work. Thus for N frequencies and M lateral wave modes, the models can be solved with a computational effort of $\mathrm{O}((M \log M)(N \log N))$ instead of the usual effort of $\mathrm{O}(M^2 N^2)$ associated with direct evaluation of the convolution sums.

In this paper we have restricted the model validation to unidirectional wave propagation. A test of relatively long waves passing a submerged bar shows that the inclusion of second-order nonlinearity gives a clear improvement of the wave shape as well as of the description of the important release of higher harmonics after the bar top. For the second test of shorter waves, the second-order effects on the wave profiles are most evident on the bar top, again leading to improved results for the second-order models, but cumulative phase errors due to an over-prediction of the amplitude dispersion have been observed as well. For both simulations results of the 'exact' and 'resonant' models showed only small deviations.

The over-prediction of the amplitude dispersion has been investigated further through a third-order Stokes-type analysis of the equations. For the 'exact' model formulated in the wave amplitudes, the third-order transfer is over-predicted from shallow to deep water, the over-prediction being more than a factor of 2 in the deep water limit. For a zero net mass flux, the model formulated in η over-predicts the amplitude dispersion with up to a factor of 5 in intermediate water. If, alternatively, the reference solution for a zero mean Eulerian velocity below wave trough level is used for comparison, the over-predictions is smaller, i.e., around a factor of 2 at maximum for the 'exact' model formulated in η. The models formulated in ϕ shows over-prediction of the amplitude dispersion and third-order transfer at intermediate depth, decaying to zero at deep water. For both third-order properties investigated, the effect of the resonance approximation has been found small.

While the derivation of fully dispersive evolution equations with exact second-order transfer is a worthwhile theoretical result, the restriction of the FFT speed-up to the 'resonant' models, makes these 'resonant' models the attractive choice for practical use. The present results show that for unidirectional wave propagation the practical difference between the 'exact' and 'resonant' models is small. A further investigation of the differences for two-dimensional wave propagation is therefore an interesting next step. The strong over-prediction of the amplitude dispersion is a new finding that restricts the application area of the models to wave fields where third-order effects are unimportant or to frequency ranges away from the region of strong over-prediction. A full inclusion of third-order terms would fix the problem but seems infeasible if the numerical efficiency is to be retained. However, an approximate correction term may help on the third-order problems. Such a correction would extend the scope of the models and ongoing research is investigating this matter.

Acknowledgements

This work was financially supported by the Danish Technical Research Council (STVF grant no. 9801635). This support is greatly appreciated. Inspiring discussions with Tim Janssen, TU Delft, are gratefully acknowledged.

References

[1] V.E. Zakharov, Stability of periodic waves of finite amplitude on the surface of a deep fluid, J. Appl. Mech. Tech. Phys. 9 (1968) 190–194 (English translation).
[2] Y. Liu, D.K.P. Yue, On generalized Bragg scattering of surface waves by bottom ripples, J. Fluid Mech. 356 (1998) 297–326.
[3] O.M. Phillips, The Dynamics of the Upper Ocean, second ed., Cambridge University Press, 1977.
[4] M.H. Freilich, R.T. Guza, Nonlinear effects on shoaling surface gravity waves, Philos. Trans. Roy. Soc. London A 311 (1984) 1–41.
[5] P.L.-F. Liu, S.B. Yoon, J.T. Kirby, Nonlinear refraction–diffraction of waves in shallow water, J. Fluid Mech. 153 (1985) 185–201.
[6] S.B. Yoon, P.L.-F. Liu, Interactions of currents and weakly nonlinear water waves in shallow water, J. Fluid Mech. 205 (1989) 397–419.
[7] P.A. Madsen, O.R. Sørensen, Bound waves and triad interactions in shallow water, Ocean Engrg. 20 (1993) 359–388.
[8] Y. Chen, P.L.-F. Liu, Modified Boussinesq equations and associated parabolic models for water wave propagation, J. Fluid Mech. 288 (1995) 351–381.
[9] J.M. Kaihatu, J.T. Kirby, Two-dimensional parabolic modelling of extended Boussinesq equations, J. Waterway Port Coastal Ocean Engrg. 127 (1998) 57–67.
[10] Y. Agnon, A. Sheremet, J. Gonsalves, M. Stiassnie, Nonlinear evolution of a unidirectional wave field, Coastal Engrg. 20 (1993) 29–58.
[11] J.M. Kaihatu, J.T. Kirby, Nonlinear transformation of waves in finite water depth, Phys. Fluids 7 (8) (1995) 1903–1914.
[12] Y. Eldeberky, P.A. Madsen, Deterministic and stochastic evolution equations for fully dispersive and weakly nonlinear waves, Coastal Engrg. 38 (1999) 1–24.
[13] J. Sharma, R. Dean, Second-order directional seas and associated wave forces, Soc. Petroleum Engrg. J. (1981) 129–140.
[14] H. Bredmose, H.A. Schäffer, P.A. Madsen, Boussinesq evolution equations: Numerical efficiency, breaking and amplitude dispersion, Coastal Engrg. 51 (11–12) (2004) 1117–1142.
[15] S. Beji, J.A. Battjes, Experimental investigation of wave propagation over a bar, Coast. Engrg. 19 (1993) 151–162.
[16] Y. Agnon, A. Sheremet, Stochastic nonlinear shoaling of directional spectra, J. Fluid Mech. 345 (1997) 79–99.
[17] R. Dalrymple, J. Kirby, Models for very wide-angle water waves and wave diffraction, J. Fluid Mech. 192 (1988) 33–50.
[18] R.W. Whalin, The limit of applicability of linear wave refraction theory in a convergence zone, Tech. Rep. H-71-3. U.S. Army Corps of Engrs, Waterways Expt. Station, Vicksberg, MS, 1971.
[19] H. Mase, J.T. Kirby, Hybrid frequency domain KdV equation for random wave transformation, in: Proceedings of 23rd International Conference on Coastal Engineering, ASCE, 1992, pp. 474–487.
[20] J.M. Kaihatu, Improvement of parabolic nonlinear dispersive wave model, J. Waterway Port Coastal Ocean Engrg. 127 (2) (2001) 113–122.
[21] P.A. Madsen, H.A. Schäffer, Higher-order Boussinesq-type equations for surface gravity waves: Derivation and analysis, Philos. Trans. Roy. Soc. London Ser. A 356 (1998) 3123–3184.
[22] Y. Agnon, P.A. Madsen, H.A. Schäffer, A new approach to high-order Boussinesq models, J. Fluid Mech. 399 (1999) 319–333.
[23] C.C. Mei, Resonant reflection of surface water waves by periodic sandbars, J. Fluid Mech. 152 (1985) 315–335.
[24] Y. Agnon, Linear and nonlinear refraction and Bragg scattering of water waves, Phys. Rev. E 59 (2) (1999) 1319–1322.
[25] R. Dalrymple, K.D. Suh, J. Kirby, J.W. Chae, Models for very wide-angle water waves and wave diffraction. II. Irregular bathymetry, J. Fluid Mech. 201 (1989) 299–322.
[26] K.D. Suh, R. Dalrymple, J. Kirby, An angular spectrum model for propagation of Stokes waves, J. Fluid Mech. 221 (1990) 205–232.
[27] A.C. Radder, On the parabolic equation method for water-wave propagation, J. Fluid Mech. 95 (1) (1979) 159–176.
[28] C.C. Mei, The Applied Dynamics of Ocean Surface Waves, Wiley, New York, 1983.
[29] H.A. Schäffer, C.M. Steenberg, Second-order wavemaker theory for multidirectional waves, Ocean Engrg. 30 (2003) 1203–1231.
[30] C. Canuto, M.Y. Hussaini, A. Quarteroni, T.A. Zang, Spectral Methods in Fluid Dynamics, Springer, New York, 1987.
[31] B.M. Sumer, J. Fredsøe, Hydrodynamics Around Cylindrical Structures, Advanced Series on Ocean Engineering, vol. 12, World Scientific, 1997.
[32] J.D. Fenton, A fifth-order Stokes theory for steady waves, J. Waterway Port Coastal Ocean Engrg. 111 (2) (1985) 216–234.